Master Thesis

Sparse Channel Estimation based on Compressed Sensing Theory for UWB systems

By

Eva Lagunas Targarona
eva.lagunas@upc.edu

Advisor: Prof. Montserrat Nájar Martón
montse.najar@upc.edu

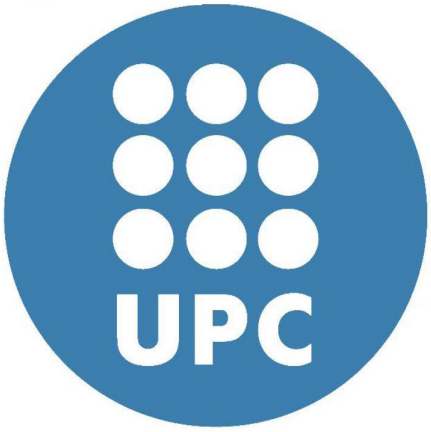

European Master of Research on Information and Communication Technologies (MERIT)
Department of Signal Theory and Communications (TSC)
Universitat Politencnica de Catalunya (UPC)

Barcelona, November 2010

Typeset in LaTeX 2_ε.

Except where acknowledged in the customary manner, the material presented in this thesis is, to the best of my knowledge, original and has not been submitted in whole or part for a degree in any university.

Eva Lagunas Targarona

Abstract

Title: Sparse Channel Estimation based on Compressed Sensing Theory for UWB Systems.
Author: Eva Lagunas Targarona
Department: Signal Theory and Communications
Supervisor: Prof. Montserrat Nájar Martón

Abstract:

In recent years, the wireless revolution has become a reality. Wireless is everywhere having significant impact on our lifestyle. However, wireless will never have the same propagation conditions as wires due to the harsh conditions of the wireless propagation. The mobile radio channel is characterized by multipath reception, that is the signal offered to the receiver contains not only a direct line-of-sight radio wave, but also a large number of reflected radio waves. These reflected waves interfere with the direct wave, which causes significant degradation of the performance of the link. A wireless system has to be designed in such way that the adverse effect of multipath fading is minimized. Fortunately, multipath can be seen as a blessing depending on the amount of Channel State Information (CSI) available to the system. However, in practise CSI is seldom available a priori and needs to be estimated.

On the other hand, a wireless channel can often be modeled as a sparse channel in which the delay spread could be very large, but the number of significant paths is normally very small. The prior knowledge of the channel sparseness can be effectively use to improve the channel estimation using the novel Compressed Sensing (CS) theory.

CS originates from the idea that is not necessary to invest a lot of power into observing the entries of a sparse signal because most of them will be zero. Therefore, CS provides a robust framework for reducing the number of measurement required to summarize sparse signals.

The sparse channel estimation here is focused on Ultra-WideBand (UWB) systems because the very fine time resolution of the UWB signal results in a very large number of resolvable multipath components. Consequently, UWB significantly mitigates multipath distortion and provides path diversity. The rich multipath coupled with the fine time resolution of the UWB signals create a challenging sparse channel estimation problem.

This Master Thesis examines the use of CS in the estimation of highly sparse channel by means of a new sparse channel estimation approach based on the frequency domain model of the UWB signal. It is also proposed a new greedy algorithm named extended Orthogonal Matching Pursuit (eOMP) based on the same principles than

classical Orthogonal Matching Pursuit (OMP) in order to improve some OMP characteristics. Simulation results show that the new eOMP provides lower false path detection probability compared with classical OMP, which also leads to a better TOA estimation without significant degradation of the channel estimation. Simulation results will also show that the new frequency domain sparse channel model outperforms other models presented in the literature.

Keywords: Channel estimation, Ultra-WideBand, Compressed Sensing, Orthogonal Matching Pursuit.

Acknowledgements

First and foremost, I would like to thank to my thesis advisor, Prof. Montse Nájar for introducing me to the world of research and for being a helpful guide during my first steps in the field.

I am very grateful for the scholarship I received during my studies, which helped me immensely in allowing me to focus on my research. I would like to express my gratitude to my Scholarship FI-DGR 2010 from Generalitat de Catalunya for financing my studies.

I am thankful to my colleagues at the UPC and to my friends in Terrassa for reminding me day after day that not everything in life is work and research.

Finally, thanks so much to my family for encouraging me: grandparents Francisco and Pepita, my parents Miguel Angel and Montse, my sister Anna, her husband Oriol and my lovely nephew Jac. I would also like to thank my family from Madrid. And my special thanks go to Inaki.

List of Publications

- E. Lagunas, M. Nájar, *Sparse Channel Estimation based on Compressed Sensing Theory for UWB Systems* (submitted to Int. Conf. on Acoustics, Speech and Signal Processing, Prague, Czech Republic, May 22-27, 2011).

Notation

Boldface upper-case letters denote matrices and boldface lower-case letters denote column vectors.

$\mathbb{R}$,$\mathbb{C}$	The set of real and complex numbers, respectively.
$\mathbb{R}^{n\times m}$,$\mathbb{C}^{n\times m}$	The set of $n \times m$ matrices with real- and complex-valued entries, respectively.
$\mathbf{A}^*$	Complex conjugate of the matrix $\mathbf{A}$.
$\mathbf{A}^T$	Transpose of the matrix $\mathbf{A}$.
$\mathbf{A}^H$	Complex conjugate and transpose (hermitian) of the matrix $\mathbf{A}$.
arg	Argument.
max,min	Maximum and minimum.
$\lvert a\rvert$	Modulus of the complex scalar a.
$\lVert\mathbf{a}\rVert$	Euclidean norm of the vector $\mathbf{a}$: $\lVert\mathbf{a}\rVert = \sqrt{\mathbf{a}^H\mathbf{a}}$.
$\lVert\mathbf{a}\rVert_p$	p-norm of the vector $\mathbf{a} \in \mathbb{C}^{n\times 1}$: $\lVert\mathbf{a}\rVert_p = (\sum_{i=1}^{n} \lvert a_i\rvert^p)^{1/p}$.
π	Pi $\pi = 3.1416$.
j	Imaginary unit $j = \sqrt{-1}$.
$\delta(t)$	Dirac delta function.

Acronyms

ADC Anaolog-to-Digital Converter

AIC Analog-to-Information Converter

AWGN Additive White Gaussian Noise

BP Basis Pursuit

ECC Electronic Communications Committee

CS Compressed Sensing

CSI Channel State Information

DSP Digital Signal Processing

eOMP Extended Orthogonal Matching Pursuit

FCC Federal Communications Commission

FFT Fast Fourier Transform

IEEE Institute of Electronical and Electrics Engineers

IFFT Inverse Fast Fourier Transform

i.i.d. Independent and Identically Distributed

JPEG Joint Photographic Experts Group

LOS Line of Sight

LP Linear Program

LS Least Squares

ML Maximum Likelihood

MP Matching Pursuit

MPC MultiPath Components

MRC Maximal Ratio Combining

OMP Orthogonal Matching Pursuit

RIP Restricted Isometry Property

RMSE Root Mean Squared Error

SNR Signal to Noise Ratio

UWB Ultra WideBand

vs versus

WPAN Wireless Personal Area Network

Contents

List of Figures

1

Motivation, Objectives and Structure

1.1 Motivation

Wireless communications systems have advanced significantly in the past years and played an extremely important role in our society. The demand for communications among people is increasing exponentially, requiring more connectivity, more services, and higher quality.

Wireless communication is the transfer of information without the use of wires, allowing the user the freedom to be mobile. Apart from user satisfaction, there is a very legitimate justification of wireless connectivity from the service providers point of view. There are many areas in the world that are still inaccessible to land line systems due to their remoteness or because of intervening inhospitable terrain. In addition, the economic point of view has also helped in the success of wireless communications. At the beginning, the mobile devices get a little market penetration due to the high cost and the technological challenges involved. But in the last thirty years, cellular telephony alone has been growing at rates similar to that of television and the automobile. Having this in mind, it is easy to guess that wireless communications holds enough promise to be the technology that drives our lifestyle and indeed our culture into the next millenium. However, skeptics will point out that wireless will never deliver the same maximum bandwidth as wires, cables or fiber-optics due to the harsh conditions of the wireless propagation. Every wireless system has to combat transmission and propagation effects that are substantially more hostile than for a wired system.

Reflection, diffraction and scattering from surrounding objects are typical effects suffered by signals while propagate through a wireless channel. Because of this effects, the transmitted signal arrives at the receiver as a supperposition of multiple attenuated and delayed copies of the original signal. This multipath leads to fading, which is one of the most important factors when designing receivers. However, multipath can be

seen both as a curse or as a blessing from a communications point of view depending on the amount of Channel State Information (CSI) available to the system. If the channel characteristics are known at the receiver, it can be effectively use to improve the communications performance.

Channel estimation algorithms allow the receiver to approximate the impulse response of the channel. This knowledge of the channel's behavior is well-utilized in modern radio communications. Adaptive channel equalizers utilize channel estimates to overcome the effects of inter symbol interference. Diversity techniques (for e.g. Rake receiver) utilize the channel estimate to implement a matched filter such that the receiver is optimally matched to the received signal instead of the transmitted one. Maximum likelihood detectors utilize channel estimates to minimize the error probability.

From the physical layer point of view, the goal is to devise schemes and techniques that increase the information rate and improve the robustness of a communication system under the harsh conditions of the wireless environment.

On the other hand, Ultra WideBand (UWB) communications [3]-[4] has emerged as a promising technology for wireless communications. Designed for low-power, short-range, wireless personal area networks (WPANs), UWB is the leading technology for freeing people from wires, enabling wireless connection of multiple devices for transmission of video, audio and other high-bandwidth data. The transmision of ultrashort pulses (on the order of nanoseconds) in UWB leads to several desirable characteristics such as the rich multipath diversity introduced by the large number of propagation paths existing in a UWB channel. The rich multipath coupled with the fine time resolution of UWB create a challenging channel estimation problem. Fortunately, multipath wireless channels tend to exhibit impulse responses dominated by a relatively small number of clusters of significant paths, especially when operating at large bandwidths [5]. Our intuition tells us that conventional channel estimation methods will provide higher errors because they ignore the prior knowledge of the sparseness.

1.2 Objectives

In this research work, channel estimation in UWB systems is investigated. The main objective of this thesis is to investigate the performance of channel estimation in UWB systems based on the new Compressed Sensing theory [6]-[7] using a frequency domain sparse model of the received signal. The resulting accurate channel state information can be used in the receiver in order to increase the robustness. Due to the energy dispersion, a robust receiver that is capable of collecting the rich multipath will mitigate performance degradation.

It will be shown that the sparse channel estimation can be obatined from a set of compressed samples obtained from an analog-to-information conversion (AIC) (an alternative to conventional ADC) applying sparse signal reconstruction techniques. There are many approaches discussed in literature for sparse signal recovery from linear measurements. The study here is focused in Orthogonal Matching Pursuit (OMP) [8], a fast and efficient greedy algorithm. However, imperfections between the assumed

model and the received signal will cause false path detection. This false path detection leads to a wrong TOA estimation. To improve the TOA estimation but preserving the performance of the channel estimator it is proposed an extended OMP (eOMP).

The objective is to proof that the new sparse model can outperform other models present in the literature and that the new eOMP algorithm is able to improve the TOA estimation without degrading the sparse channel estimation obtained with classical OMP.

1.3 Structure of the Thesis

The reminder of this thesis is organized as follows:

Chapter 2 introduces the Compressed Sensing theory following [6] and [7]. The notation is briefly summarized and the most widely used sparse signal recovery algorithms are explained. Then, a general Ultra WideBand (UWB) background, without too many equations, is presented. Finally, a channel estimation introduction with some references of the state of the art is given.

In **Chapter 3** and **Chapter 4** there are the major contribution of this thesis. In **Chapter 3** the new frequency domain sparse model of the UWB signal and the extended OMP are presented with detail. Simulations are given in **Chapter 4**. Results are discussed for different compression rates, comparing the classic OMP with the new eOMP and comparing the new model with the previous ones present in the literature.

Finally, in **Chapter 5** the conclusions are drawn and further work is proposed.

2 Introduction

2.1 Compressed Sensing

Signal acquisition is a main topic in signal processing. Sampling theorems provide the bridge between the continuous and the discrete-time worlds. The most famous theorem is often attributed to Shannon [9] (but usually called Nyquist rate) and says that the sampling rate must be twice the maximum frequency present in the signal in order to perfectly recover the signal. In the field of data conversion, standard analog-to-digital converter (ADC) technology implements the usual quantized Shannon representation: the signal is uniformly sampled at or above the Nyquist rate.

However, as David L. Donoho said: *The sampling theory is wrong; not literally wrong but psychologically wrong.* This Master Thesis surveys the theory of Compressive Sampling, also known as Compressed Sensing (CS), a novel sampling paradigm that goes further than Shannon's theorem. The idea is to perfectly recover the signal using far fewer samples of measurements than traditional methods. CS allows to compress the data while is sampled. It originates from the idea that it is not necessary to invest a lot of power into observing the entries of a sparse signal because most of them will be zero. Considering a sparse signal, it should be possible to collect only a small number of measurements that still allow for reconstruction.

As it is explained in [6] most of the data acquired by modern systems and technologies can be thrown away with almost no perceptual lost. This phenomenon raises very natural questions: why to acquire all the data when most of that will be thrown away? why don't we try to just directly mesure the part that will not be thrown away?

CS methods provide a robust framework for reducing the number of measurement required to summarize sparse signals. Is for that reason that CS is usefull in systems where the analog-to-digital conversion is critical, for example UltraWideBand (UWB) systems.

2.1.1 Review of Compressed Sensing

In the last years, thousands studies of sparse representation and compressive sensing have been published, specially in the signal processing community. A tutorial overview of some of the foundational developments in CS can be found in [7]-[10]. In order to briefly review the main ideas of CS, consider the following real-valued, finite length, discrete time signal $x \in \mathbb{R}^M$ which can be expressed in an orthonormal basis $\Psi = [\psi_1 \psi_2 ... \psi_M]$ as follows:

$$\mathbf{x} = \sum_{i=1}^{M} \psi_i \theta_i \tag{2.1}$$

where the vector $\theta = [\theta_1 \theta_2 ... \theta_M]$ is a sparse vector, which means that is a vector with very few non-zero components. Using matrix notation it may be respresented as

$$\mathbf{x} = \Psi\theta \tag{2.2}$$

where matrix Ψ has dimension $M \times M$. A vector with only K non-zero components will be called from now on *K-sparse* vector in that particular basis.

2.1.2 Sparsity

Sparsity expresses the idea that the information rate of a continuous time signal may be much smaller than suggested by its bandwidth, or that discrete-time signal depends on a number of degrees of freedom which is comparably much smaller than its length [7].

Many signals are sparse if they are expressed in a convenient basis. The implication of sparsity is that one can discard the part of the coefficients without much perceptual loss. Thus, it is not necessary to invest a lot of power into observing the entries of a sparse signal in all coordinates when most of them are zero anyway. This principle is applied for example in JPEG coders [11]. Such process requires not only the knowledge of the M coefficients of θ but also the locations of the significant pieces of information. Fortunately for us, these significant information tend to be clustered. As an example of sparse-clustered model, it has been shown that many physical channels tends to be distributed as clusters within respective channel spreads [12].

The sparsity is one of the constraints required for the reconstruction process.

- *Sparsity*: The signal $\mathbf{x}$ should be sparse in the basis Ψ. It means that $\mathbf{x}$ can be represented using only a small number $K << M$ of atoms from Ψ.

$$\|\Psi\mathbf{x}\|_{l_0} \leq K \tag{2.3}$$

The theory extends to signals that are well approximated with a signal that is K-Sparse in Ψ.

2.1.3 Sensing and Incoherence definition

As it was said before, when applying CS theory to communications, the sampling rate can be reduced to sub-Nyquist rate. Consider the classical linear measurement model for the above signal,

$$\mathbf{y} = \Phi\mathbf{x} = \Phi\Psi\theta \tag{2.4}$$

where $\Phi\Psi$ form the effective measurement matrix for estimating the *K-sparse* vector θ. Matrix Φ is called measurement matrix and it has rank N lesser than the rank of the signal $\mathbf{x}$ which is equal to M. The $N \times M$ matrix Φ is projecting the signal $\mathbf{x}$.

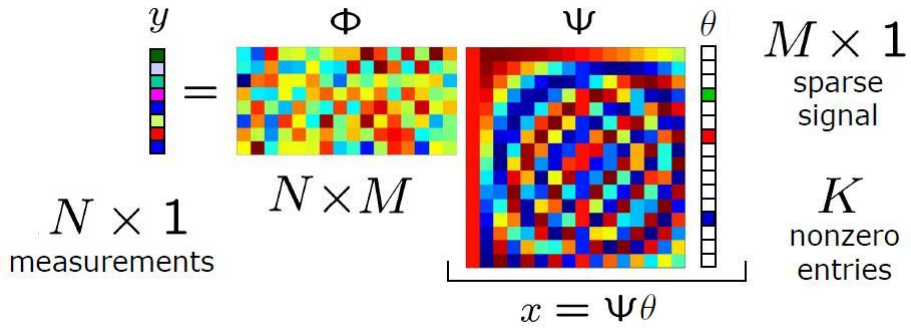

FIGURE 2.1: Compressed Sensing: Mathematical Respresentation

The incoherence is defined as the maximum value amongst inner product of the orthonormal basis and the orthonormal measurement matrix. A low value of incoherence is desirable in order to ensure mutually independent matrices and therefore better compressive sampling. The coherence can be measured as

$$\mu(\Phi, \Psi) = \max_{\substack{1 \le k \le N \\ 1 \le j \le M}} |\langle \phi_k, \psi_j \rangle| \tag{2.5}$$

It follows from linear algebra that the maximal incoherence is obtained when $\mu = 1$. One example of maximal incoherence is when $\phi_k(t) = \delta(t - k)$ and Ψ is the Fourier basis, $\psi_j(t) = e^{i2\pi jt/n}$. This example corresponds to the classical sampling scheme.

Finally, only remark that random matrices are largely incoherent with any fixed matrix Ψ.

2.1.4 Sparse Signal Recovery

Restricted Isometry Property

The problem in CS consist of designing a convenient measurement matrix such that salient information in any compressible signal is not damaged by the dimensionality reduction and designing a reconstruction algorithm to recover θ from only N compressed measurements. Remember that the sparse signal has N components and $N << M$. Both problems are represented in Fig. 2.2.

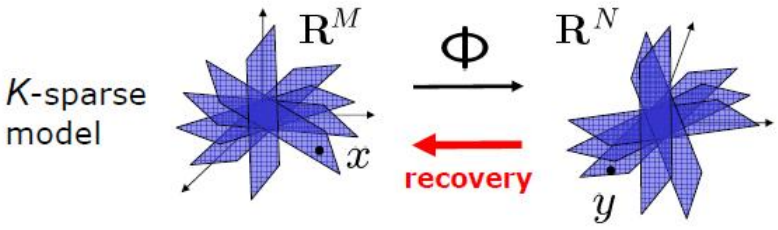

FIGURE 2.2: Sparse Signal Recovery

The most commonly used criterion for evaluating the quality of a CS measurement matrix is the restricted isometry property (RIP) introduced in [10] by Candés, Romberg and Tao (which they initially called the uniform uncertainty principle). This property can be summarized as follows,

$$(1-\delta_s)\left\|\theta\right\|_{l_2}^2 \leq \left\|\Phi\Psi\theta\right\|_{l_2}^2 \leq (1+\delta_s)\left\|\theta\right\|_{l_2}^2 \tag{2.6}$$

for a particular positive constant δ_s. Here $\left\|\cdot\right\|_{l_2}^2$ denotes the l_2-*norm* of a vector. This condition must be satisfied by Φ in order to successfuly recover the signal. Fortunately again, RIP can be achieved with high probability by selecting Φ as a random matrix. It was shown that Gaussian, Bernoulli and partial random Fourier matrices [13] possess this important property.

If the RIP holds , then it is shown in [14] that the following linear program gives an accurate reconstruction:

$$\min_{\theta^* \in \mathbb{R}^M} \left\|\theta^*\right\|_{l_1} \quad s.t. \quad \mathbf{y} = \Phi\Psi\theta^* \tag{2.7}$$

where $\left\|\theta\right\|_{l_1} = \sum_{i=1}^{M} |\theta_i|$.

Theorem 1. ([14]) *Assume that θ is K-sparse and that we are given N Fourier coefficients with frequencies selected uniformly at random. Suppose that the number of observations obeys,*

$$N \geq c \cdot K \cdot \log M/K \tag{2.8}$$

Then minimizing l_1 reconstructs θ exactly with overwhelming probability. In details, if the constant c is of the form $22(\delta+1)$ in (2.8), then the probability of success exceeds $1 - O(M^{-\delta})$.

Signal Reconstruction Algorithms

The RIP provides the theoretical basis to not damage the compressed samples, but it does not tell us how to recover the sparse vector.

Since $N << M$, there are infinitely many solutions θ^* that satisfy: $\mathbf{y} = \Phi\Psi\theta$. This reconstruction problem is usually solved by using least norm procedures. The

most common approach to solve it involves Euclidean norm (l_2 norm) for which an analytical solution exists and is given by,

$$\theta^* = (\Phi\Psi)^H((\Phi\Psi)(\Phi\Psi)^H)^{-1}\mathbf{y} \tag{2.9}$$

In most cases least-norm solution with Euclidean norm gives very poor results: solution is almost never sparse. The result is improved by using the sparse prior information. If we know a priori that our original signal θ is sparse, then a natural choice would be to find a vector with least non-zero entries. This is called l_0 norm.

$$\min_{\theta^* \in \mathbb{R}^M} \|\theta^*\|_{l_0} \quad s.t. \quad \mathbf{y} = \Phi\Psi\theta^* \tag{2.10}$$

Note that $\|\cdot\|_{l_0}$ is not a norm by definition, but is known as *quasi-norm*. Unfortunately, this problem requires an exhaustive search and, in general, it is not a feasible problem. In general, the equality constraint can be relaxed (more details in [15]).

Surprisingly, Candes and Donoho have shown in their respective works in [16] and [6] that from $N \geq cK\log(M/K)$ i.i.d. Gaussian measurements it can be exactly reconstruct K-sparse vectors and closely approximate compressible vectors with high probability via l_1 optimization.

$$\min_{\theta^* \in \mathbb{R}^M} \|\theta^*\|_{l_1} \quad s.t. \quad \mathbf{y} = \Phi\Psi\theta^* \tag{2.11}$$

The l_1-minimization is a convex program and can be recast as a linear program (LP) [3] and solved using any modern optimization technique [17]. When (2.11) is conveniently reduced to a linear program it is known as Basis Pursuit (BP) [3]. Another practical and tractable alternative proposed in the literature based on the convex relaxation leading to l_1-minimization is Matching Pursuit (MP), which use a sub-optimal greedy sequential solver [18]-[19]. MP is the current most popular algorithm for computing sparse signal reconstruction and is used in a variety of applications [20] [21].

MP begins with an empty representation (meaning a vector of zeros) and at each iteration augments the current representation by selecting the atom from the dictionary that maximally improves the representation. It is easy to implement and it ensures with high probability a relatively sparse solution.

In the general problem, the compressed samples are inaccurate measurements. In the literature there are a noise-aware variant which relaxes the data fidelity term. The reconstruction program for these kind of problems is of the form,

$$\min_{\theta^* \in \mathbb{R}^M} \|\theta^*\|_{l_1} \quad s.t. \quad \|\mathbf{y} - \Phi\Psi\theta^*\|_{l_2} \leq \epsilon \tag{2.12}$$

This problem has a unique solution, is again convex and could be solved applying convex optimization techniques. In particular, Dantzig selector [22] and combinatorial optimization programs [23] have provable results in the case of Gaussian variance-bounded noise. Problem (2.12) is often called the LASSO (Least Absolute Shrinkage and Selection Operator) [24].

Finally only mention an oversimplified situation where it is easy to see that l_1 norm fits better than l_2 norm in our problem. The complete explanation can be found in

TABLE 2.1: Signal recovery approaches

Norm	Comments
l_0-norm	Find the sparsest solution. Not feasible.
l_1-norm	Correct, efficient mild oversampling.
l_2-norm	Solution is almost never sparse.

[25]. Fig. 2.3 depict the geometry of l_1 and l_2 balls. Let us assume our original signal $\mathbf{x} \in \mathbb{R}^2$ has only one non-zero element, and we take only one measurement of that. In part (b) and (c), H denotes the line on which all possible solutions lie. To visualize how l_1 reconstruction works, imagine that we start to inflate l_1 ball from origin until it touches the line H at some point, vector at that point will be the solution. We do the same with the l_2 norm in part (c). We can see how the solution achieved in part (c) is the point on H closest to the origin, not even close to the sparse solution, which is the one achieved in part (b) by the l_1 norm. In Fig. 2.4 there is the same example in 3 dimensions. However, an interesting observation made by Michael Elad is that in many cases l_1 norm successfully finds the sparsest representation.

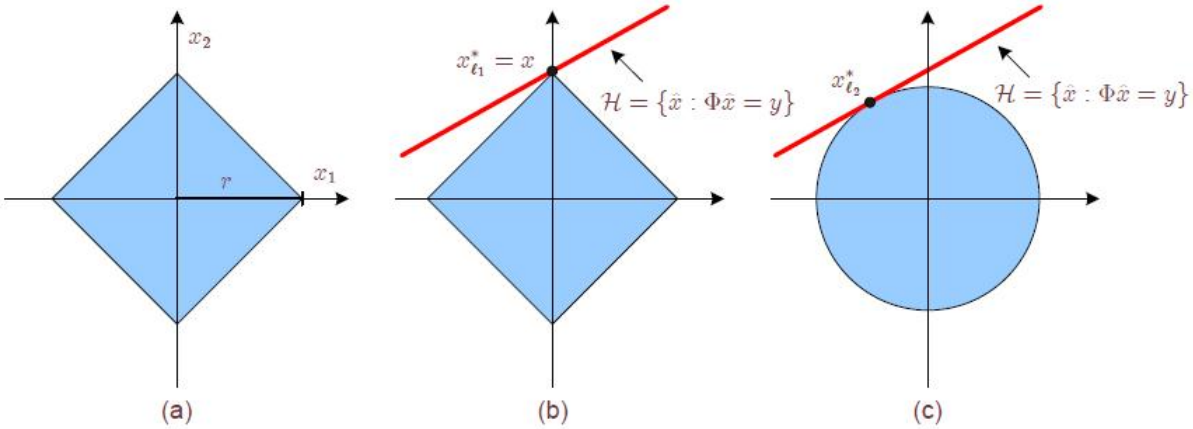

FIGURE 2.3: Geometry of l_1 minimization. (a) an l_1 ball of radius r. (b) H represents a hyperplane where all possible solutions to $\mathbf{y} = \Phi\mathbf{x}$, and l_1 ball meets the hyperplane at some vertex. (c) an l_2 ball touching H at point closest to the origin

2.1.5 Analog-to-Information Conversion: Implementation Issues

The power, stability, and low cost of digital signal processing (DSP) have pushed the analog-to-digital converter (ADC) increasingly close to the front-end of many important sensing, imaging, and communication systems. Unfortunately, many systems, especially those operating in the radio frequency (RF) bands, severely stress current

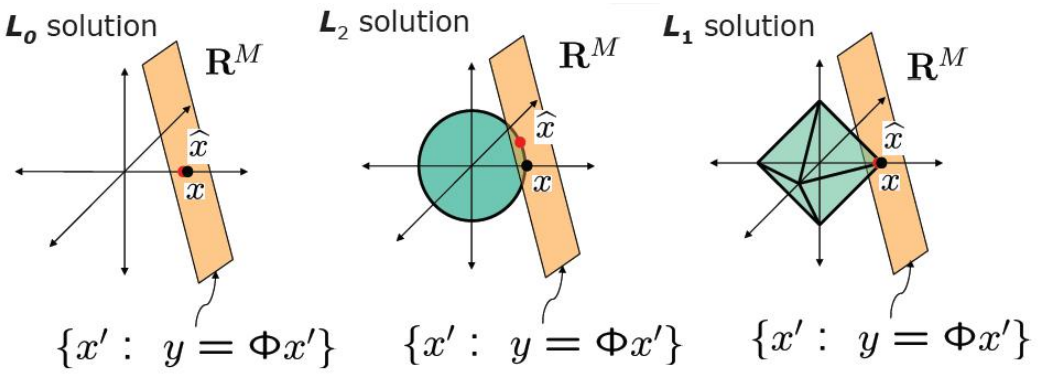

FIGURE 2.4: Geometry of l_0, l_1 and l_2 minimization

ADC technologies. Fortunately, recent developments in the CS field suggests a new framework for analog-to-information conversion (AIC) as an alternative to conventional ADC.

CS seems clear with the matrix notation, but as in many others signal processing techniques, the implementation in real systems involves certain difficulties. The implementacion and feasibility of these AIC systems is not the goal of this work. We kindly recommended [26] and [27] reading for a deepest knowledge. In [26], the feasibility of hardware implementation of a sub-Nyquist random-sampling based on analog to information converter (RS-AIC), which utilizes the theory of information recovery of wideband Locally Fourier Sparse (LFS) signals to reconstruct signals from far fewer samples than required in Shannon theorem, is successfully demonstrated. In [27] a system that uses modulation, filtering, and sampling to produce a low-rate set of digital measurements inspired by the theory of compressive sensing is proposed.

2.1.6 Applications

Compressed sensing can be potentially used in all applications where the task is the reconstruction of a signal or an image from a small set of linear measurements. Below is a list of applications where CS is currently used.

- Data Compression
- Channel Coding
- Data Acquisition
- Analog-to-Information Conversion
- Electroenecephalography (EEG)
- Optical Coherence Tomography (OCT)
- Target Detection or Radar

2.1.7 Summary

Section 2.1 describes the Compressed Sensing theory. It is shown that CS method greatly reduces the number of digital samples required to reconstruct certain sparse signals. The key ideas of this technology are presented, some mathematical support is given and many references of interest published by the most prominent authors in this topic are provided. A large collection of the vastly growing reserach literature on the subject is available on the webpage **http://www.compressedsensing.com**.

2.2 Ultra WideBand (UWB) technology

This section tries to briefly present a general Ultra WideBand (UWB) background.

Short-range wireless technology will play a key role in scenarios where everybody and everything is connected by different types of communication links. While the majority of human to human information exchanges are still by voice, a rapid increase in data transfers is observed in other types of links as manifested by the rising need for location-aware applications and video transfer capability within the home and office enviroments. UWB could play an important role in the realization of future pervasive and heterogeneous networking. The new demands on low power, low interference and high data rates makes the use of UWB an attractive option for current and future wireless applications.

2.2.1 Ultra WideBand Overview

Ultra-Wideband, or UWB as it has become known, is a term for a classification of signals that occupy a substantial bandwidth relative to their centre frequencies. The definition of UWB signals is related to the occupied frequency bandwidth. To specifically define what is meant by an UWB signal, the following fractional bandwidth definition is employed:

$$B_f = 2\frac{f_h - f_l}{f_h + f_l} \tag{2.13}$$

where f_l and f_h are the lower and upper end (3 dB points) of the signal spectrum, respectively. UWB signals are then those signals that have a fractional bandwidth greater than 25 percent. On the other hand, according to the Federal Communications Commission (FCC) [28], a UWB signal is defined to have an absolute bandwidth of at least 500 MHz. In general we can talk about UWB when referring to signals that occupy a very large portion in the spectrum. Therefore, a set of regulations are imposed on systems transmitting UWB signals. The transmitted average power spectral density must not exceed -41.3 dBm/MHz over the frequency band from 3.1 to 10.6 GHz, and it must be even lower outside this band. Fig. 2.5 illustrates the FCC limits for indoor communications systems. After the legalizationof UWB signals in USA, a considerable amount of effort has been put into development of UWB systems. Later, Japan and Europe also allowed the use of UWB under certain regulations [29].

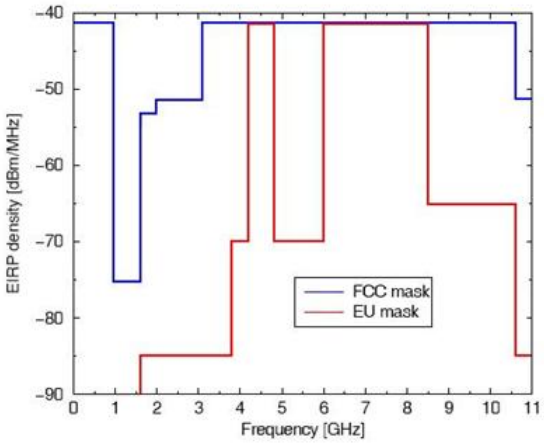

FIGURE 2.5: FCC limits for indoor UWB communications systems

The use of large transmission bandwidths offers a number of benefits, including accurate ranging, robustness to propagation fading, superior obstacle penetration, resistance to jamming, interference rejection, and coexistence with narrow bandwidth (NB) systems [30].

2.2.2 Origins

UWB radio is a field of research that is old and new at the same time. The idea of periodically sending ultra-short duration pulses is nothing new and can be dated back to 1887 when Hertz experimented with the spark gap, which was later incorporated into the telegraph by Guglielmo Marconi. The radar community has been using similar pulse signals for ground-penetration radars for many years. In the early 1990s, conferences on UWB technology were initiated and proceedings documented in book form. For the most part, the papers of these conferences are motivated by radar applications. UWB communications gained prominence with the groundbreaking work on impulse radio by Win and Scholtz [4]-[31] in the 1990s and received a major boost by the 2002 decision of the US FCC to allow unlicensed UWB operations. Since that time, an unprecedented transformation in the design, deployment, and application of short-range wireless devices and services is in progress.

2.2.3 Unique Features and Issues

UWB has a number of advantages that make it attractive for consumer communications applications. The low complexity and low cost of UWB systems arises from the essentially baseband nature of the signal transmission.

The lack of available spectrum to support the growing number of wireless devices is well known. In the short-range application space, UWB can drive potential solutions for many of today's problems identified in the areas of spectrum management. The novel approach proposed by UWB is based on optimally sharing the existing radio spectrum

resources rather than looking for still available but possibly unsuitable new bands. UWB transmissions do not cause significant interference to existing radio systems. The interference phenomenon between impulse radio and existing radio systems is one of the most important topics in current UWB research.

Due to their large bandwidth, UWB systems are characterized by very short duration waveforms, usually on the order of a nanosecond. Its large frequency spectrum that includes low frequencies as well as high frequencies results in an important penetration capability. This large spectrum also results in high time resolution, which improves the ranging accuracy.

The huge *new bandwidth* opens a door for an unprecedented number of bandwidth-demanding position-critical low-power applications in wireless communications, radar imaging, and localization systems. The Power Spectral Density (PSD) of UWB systems is generally considered to be extremely low. For UWB systems, the transmitted energy is spread out over a very large bandwidth and one of the benefits of a low PSD is a low detection probability, which is of particular interest for military applications. This is also concern for wireless consumer applications, where the security of data is considered to be insufficient. The comparison for the PSD of UWB with other systems is shown in Fig. 2.6.

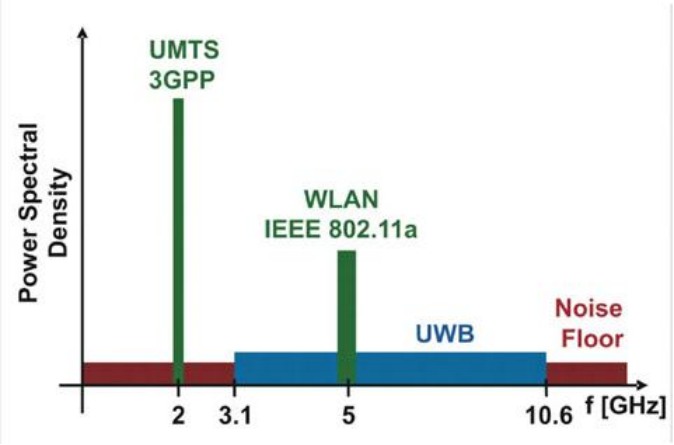

FIGURE 2.6: Low-energy density and high-energy density systems

At this point, is unavoidable to highlight the transmission speed of UWB technology. Most UWB communications transmissions are achieving the range of 100-500 MHz (which is 100 to 500 times the speed of Bluetooth, see Table. 2.3). Currently, standardization institutions are working on legislation that classifies the UWB transmission rates into three different categories (see Table 2.2).

2.2.4 TOA in UWB

One of the reasons why UWB radio is considered a viable solution for indoor localization is the great time resolution of the signal, which translates into good ranging accuracy and good ability to distinguish different arriving multi-path components (MPCs). That

TABLE 2.2: UWB bit rate

Standard	Speed (Mbps)
UWB	480
UWB (4m min)	200
UWB (10m min)	110

TABLE 2.3: Wireless standards bit rate

Standard	Speed (Mbps)
802.11a	54
802.11g	20
802.11b	11
Ethernet	10
Bluetooth	1

is why among all the parameters that have been traditionally used for positioning (received signal strength intensity (RSSI), the angle of arrival and time of arrival), the Time of Arrival (TOA) stands out as the most suitable signal parameter to be used for positioning with UWB devices. The basic problem of TOA-based techniques is to accurately estimate the propagation delay of the radio signal arriving from the direct line-of-sight (LOS) propagation path.

TOA estimation algorithms have been extensively studied these years, including those considering high sampling rate, matched filtering (MF) based coherent algorithms, and those considering lower sampling rate, energy detection based non-coherent algorithms.

TOA estimation in a multipath environment is closely related to channel estimation, where channel amplitudes and time of arrivals are jointly estimated using, for example, a maximum likelihood (ML) approach [32] [33]. Typical approaches for UWB impulse radio ranging in the literature are based on computing the correlation between the received signal and a reference signal. On a white additive Gaussian noise (AWGN) channel their TOA can be measured within the accuracy of the Cramer-Rao bound by correlating the received signal with a template waveform shaped as the transmitted pulse and looking for the time shift of the template that yields the largest correlation. However, the implementation of a correlation-based TOA estimator is practically impossible because pulse overlaps are likely to occur.

TOA estimation based on signal energy measurements is pursued in [34]. The incoming signal is squared and integrated over intervals comparable with the pulse width. The location of the first arriving path is computed as the index of the first interval where the energy overcomes a suitable threshold.

The correlation method outperforms the non-coherent algorithms, on the cost that an extreme high sampling rate is required. Accuracy in UWB TOA measurements is

linked to implementation limitations: Working with digital approaches involve analog-to-digital (ADC) converters operating in the multi-GHz range. Due to the practical limitations of the correlation based methods, energy detection based algorithms are preferred in most sensor applications. Unfortunately, the ranging precision of energy detection is mainly restricted by the threshold decision, which is based only on the noise level in traditional algorithms.

Summarizing, TOA estimation is a challenging task and is currently the focus of intense research.

2.2.5 UWB Architecture Challenges

Any practical UWB system design should take into account implementation feasibility and complexity issues.

The signal bandwidths and fractional bandwidths of UWB radio are at least an order of magnitude greater than those existing narrowband radios. In a UWB receiver, the analog-to-digital converter (ADC) can be moved almost up to the antenna, resulting in a dramatic reduction of the required analog circuitries, which often dominate the size, power and cost of a modern receiver. Critical to this design approach, however, is the ability for the ADC to efficiently sample and digitize at least at the signal Nyquist rate of several GHz. The ADC must also support a very large dynamic range to resolve the signal from the strong narrowband interferers. Currently, such ADCs are far from being practical [35]. There are numerous implementation challenges in the UWB radio. Chief among them are the extremely high sampling ADC and the wideband amplification requirements mentioned before. But other design challenges include for example the generation of narrow pulses at the transmitter and the digital processing of the received signal at high clock frequencies.

2.2.6 Channel Estimation with UWB

The impulse response of narrowband propagation channels can be represented as the sum of the contributions of the different MPCs. The model would be purely deterministic if the arriving signals consisted of completely resolvable echoes from discrete reflectors. However, in most practical cases, the resolution of the receiver is not sufficient to resolve all MPCs. A UWB channel differs in that the number of physical MPCs that make up one resolvable MPC is much smaller, due to the fine delay resolution. A categorization of impulse response that we will encounter in the subsequent section is *sparse* channel. In a *sparse* channel, MPCs arrive at time intervals that are (sometimes) larger than the inverse of the bandwidth of the considered channel. Whether a power delay profile is *sparse* or not depend on two aspects: the considered bandwidth (the larger the bandwidth, the more likely it is that the channel shows sparse structure) and the considered enviroment. Enviroments with a large number of reflecting and diffracting objects can lead to dense channels even for extremely large bandwidths.

If the channel is known at the receiver, all these resolvable copies can be combined coherently to provide multipath diversity. The rich multipath diversity of an

impulse wideband channel calls for the use of Rake receivers for significant energy capture, higher performance and flexibility. In addition, accurate multipath delays (and amplitudes) extimation is indispensable.

Currently research on non-sparse channel estimation specifically for UWB wireless systems has been conducted [33][36][37][38] extensively. Although the maximum likelyhood (ML) approach [33] produces excellent results, it is impractical since the number of parameters to estimate in a realistic UWB channel is very high. Suboptimal receivers such as the energy detectors [39] and autocorrelation receivers [40] generally take a SNR penalty in order to achieve similar performance to the coherent counterpart.

The emerging theory of compressed sensing (CS) outlines a novel strategy to jointly compress and detect a sparse signal with fewer sampling resources than the traditional method.

Compressed sensing for UWB was first proposed in [41] as a generalized likelihood ratio test receiver taking advantage of the signal structure by incorporating pilot assisted modulation. In [38], it is transformed the problem into an equivalent on-off-keying (OOK) problem by exploting the sparsity in the UWB channel structure.

The issue of sparse channel estimation will be addressed later with more detail.

2.2.7 Summary

Whilst UWB is still the subject of significant debate, there is no doubt that the technology is capable of achieving very high data rates and is a viable alternative to existing technology for WPAN; short-range, high-data-rate communications; multimedia applications, and cable replacement. Particularly in ranging and localization, UWB-IR has shown to be a promising candidate that can enable centimeter accuracy with minimal cost on the SNR. On the other hand, the rich multipath characteristic of a wireless communication system operating with sub-nanosecond pulses is another attractive feature of UWB-IR. In this section we have seen these and other advantages of UWB, focusing on channel estimation and TOA estimation applications.

2.3 Channel Estimation

In a typical scattering enviroment, a radio signal emitted from a transmitter is reflected, diffracted, and scattered from the surrounding objects, and arrives at the receiver as a superposition of multiple attenuated, delayed, and phase- and/or frequency-shifted copies of the original signal. Usually we call all these effects under one word: multipath. The superposition of multiple copies of the transmitted signal is the defining characteristic of many wireless systems [42]. In the communication comunity, multipath is both a curse and a blessing. When a signal propagates through a wireless channel, it usually suffers fluctuations in the received signal strength which can affect the rate and also the reliability of communication. On the other hand, research in the last decade has shown that multipath propagation also results in an increase in the number of degrees of freedom (DoF) available for communications which can lead to significant gains in the rate (multiplexing gain) and/or reliability (diversity gain)

of communication. Of course, the multipath information can only be used effectively depending on the amount of channel state information (CSI) available to the system.

2.3.1 Methods to Estimate the Channel

In practise, CSI is seldom available to communication systems a priori and the channel needs to be estimated at the receiver in order to exploit the benefits of additional DoF afforded by multipath propagation. The methods to estimate multipath channels at the receiver can be classified into two classes: training-based channel estimation methods and blind channel estimation methods.

Training-Based Methods

In training-based channel estimation methods, the transmitter multiplexes signals that are known to the receiver (henceforth referred to as training signals) with data-carrying signals in time, frequency, and/or code domain, and CSI is obtained at the receiver from knowledge of the training and received signals. Training-based methods require relatively simple receiver processing and often lead to decoupling of the data-detection module from the channel-estimation module at the receiver, which reduces receiver complexity even further. See [43] for an overview of training-based approaches to channel estimation.

Blind Methods

In blind channel estimation methods, CSI is adquired at the receiver by making use of the statistics of data-carrying signals only. Although it is theoretically feasible, blind estimation methods typically require complex signal processing at the receiver and often entail inversion of large data-dependent matrices, which also makes them highly prone to error propagation in rapidly varying channels. See [44] for an overview of blind methods to channel estimation.

2.3.2 Sparse Channel Estimation

Experimental studies undertaken in the recent past have shown though that wireless channels associated with a number of scattering enviroments tend to exhibit sparse structures at high signal space dimension in the sense that majority of the channel DoF end up being either zero or below the noise floor when operating at large bandwith and symbol durations and/or with large plurality od antennas. See [45] for the wideband case and see [46] for the MIMO case.

Our intuition tells us that conventional channel estimation methods will provide higher errors because they ignore the prior knowledge of the sparseness. In this case, our intuition was not wrong and there are several publications that prove that [47].

The research in wireless communications, in particular the area of sparsity in channel estimation has a history that takes back to the early 1990s. Firstly, the problem of sparse-channel estimation was first faced in the context of underwater acoustic communications using training-based methods. In underwater communications only few

echoes are dominant and recursive least squares estimation can be applied ignoring the weakest dimension of the channel. Later, inspired by the fact that digital television channels and broadband channels in hilly terrains also exhibit sparse structures, Cotter and Rao proposed a sparse-channel estimation method based on the Matching Pursuit [48]. In contrast to the MP-based approach, Raghavendra and Giridhar proposed a modified Least-Squares (LS) estimator in [49] which uses a generalized Akaike information criterion to estimate the locations of non-zero channel taps.

A wireless channel can often be modeled as a sparse channel in which the delay spread could be very large, but the number of significant paths is normally very small. We can start with the basic assumption that when a short duration pulse (high frequency, for example UWB technology) propagate through multipath channels, the received signal remain sparse in some domain and thus compressed sensing is indeed aplicable. To illustrate this concept, consider the 8th order Butterworth pulse typicaly used in the UWB Standards as the information carrier pulse having a duration of $T_p = 1$ns. Fig. 2.7 shows the received signal per frame for a UWB channel that models an indoor residential enviroment with Line-Of-Sight (LOS) (according to the IEEE 802.15.4a channel model CM1 [50]) in the absence of noise.

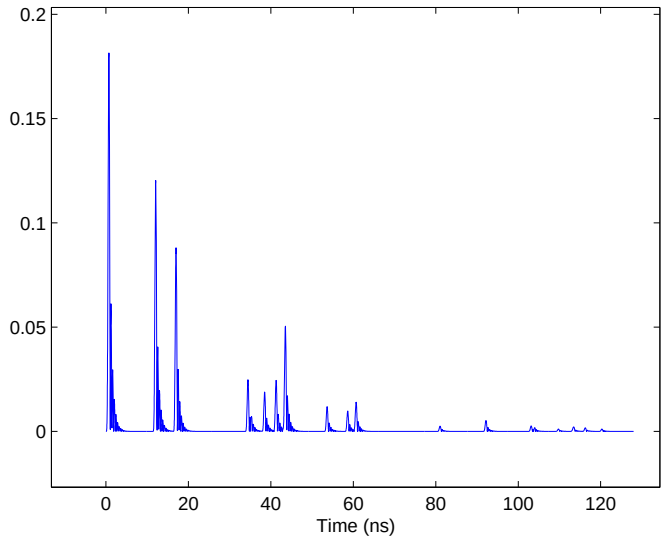

FIGURE 2.7: Effect of UWB channel indoor propagation in residential enviroment (LOS)

As is depicted in Fig. 2.7, the received signal is composed of sets of spaced clusters of the transmitted pulse. It can also be seen relatively long time intervals between clusters and rays where the signal takes zero or negligible values. In this particular example, the signal plotted in Fig. 2.7 has 12.672 taps, of which 9.765 have amplitude lower than 10^{-5}.

Existing Techniques

Existing techniques for sparse channel estimation can be categorized into two types. First of all, there are algorithms which are approximation schemes that solve the non-linear optimization problem of minimizing the squared residual error as a function of the gain and the delay location of all the dominant paths [51]. This means that optimization is carried out jointly in all coefficients. Algorithms of the second type sequentially choose the most important taps of the sampled channel impulse response. Among the techniques to do that are the L_p-norm regulized method [52] and greedy algorithms such as Matching Pursuit (MP) algorithm [48] and its orthogonal version OMP [8].

Currently, the two most popular approaches are MP [48] and basis pursuit (BP) [3]. With MP (and one of its variants OMP) the sparse signal is iteratively built up by selecting the atom that maximally improves the representation at each iteration. On the other hand, BP directly looks for the vector that minimizes the l_1-norm coefficients, which is computationally expensive. In this thesis, simulations are focused on OMP [8], which achieves faster and more efficient reconstruction.

More information about the sparse recovery methods are available in Section 3.3.

2.4 Summary

Three topics are studied in this thesis: channel estimation, compressed sensing and UWB. UWB technology has been chosen as a framework because of its high time resolution and multipath immunity. Channel estimation is faced under the compressed sensing point of view. Exploiting the sparseness of the channel the classical channel estimation approches can be improved. An overview of the three topics has been explained in this Chapter emphasizing the most important concepts that will be most used in the following chapters.

3

Frequency domain Sparse Channel Estimation

Channel estimation for purposes of equalization is a long standing problem in signal processing. Wireless propagations are characterized by sparse channels, that is channels whose time domain impulse response consists of a large number of negligible time intervals. This chapter examines the use of compressed sensing, an emerging theory for sparse signals, in the estimation of highly sparse channels. In particular, a new channel sparse model for UWB communication systems based on the frequency domain signal model is developed. It is also proposed an extended OMP (eOMP) that improves the TOA estimation without significantly degrading the channel estimation obtained with classical OMP.

3.1 UWB Signal Model

The transmitted UWB signal model can be written as,

$$s(t) = \sum_{k=0}^{\infty} \sum_{j=0}^{N_f-1} a_k p(t - jT_f - kT_{sym}) \tag{3.1}$$

where the data $a_k \in \pm 1$ is the k-th transmitted bit, T_{sym} is the symbol duration and $T_f = T_{sym}/N_f$ is the pulse repetition period. To simplify notation, in the following it is assumed $a_k = 1$. The mother pulse $p(t)$ is depicted in Fig. 3.1.

Signal $s(t)$ propagates through an L-path fading channel whose response to $p(t)$ is $\sum_{l=0}^{L-1} h_l p(t - \tau_l)$. Note that it is assumed that the received pulse from each l-th path exhibits the same waveform but experiences a different fading coefficient, h_l, and a different delay, τ_l. Without loss of generality we assume $\tau_0 \leq \tau_1 \leq \ldots \leq \tau_{L-1}$. In Fig. 3.2 is shown the resulting signal when a pulse propagates through an especific channel.

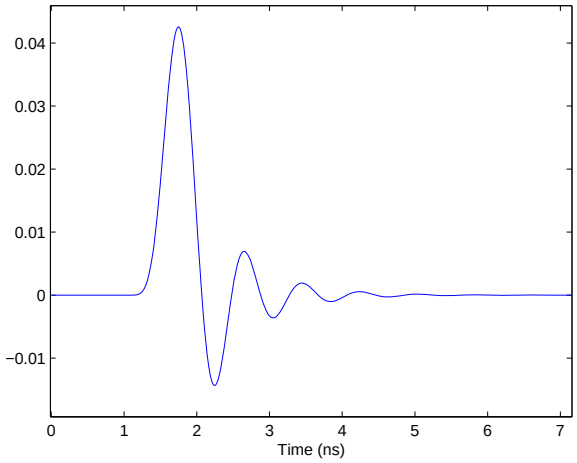

FIGURE 3.1: UWB Pulse

The received waveform can be written as

$$r(t) = \sum_{k=0}^{\infty} \sum_{j=0}^{N_f-1} \sum_{l=0}^{L-1} h_l p(t - T_k^j - \tau_l) + w(t) \tag{3.2}$$

where $w(t)$ is thermal noise with two-sided power spectral density $No/2$ and $T_k^j = jT_f + kT_{sym}$.

The signal associated to the j-th transmitted pulse corresponding to the k-th symbol, in the frequency domain yields

$$Y_j^k(w) = \sum_{l=0}^{L-1} h_l S_j^k(w) e^{-jw\tau_l} + V_j^k(w) \tag{3.3}$$

with

$$S_j^k(w) = P(w) e^{-jw(kN_f+j)T_f} \tag{3.4}$$

where $P(w)$ denotes the Fourier Transform of the pulse $p(t)$ and $V_j^k(w)$ is the noise in the frequency domain associated to the j-th frame interval correspondig to the k-th symbol. Sampling (3.3) at $w_m = w_0 m$ for $m = 0, 1, \ldots, M-1$ where $w_0 = \frac{2\pi}{T_f}$ and rearranging the frequency domain samples $Y_j^k[m]$ into the vector $\mathbf{Y}_j^k \in \mathbb{C}^{M\times 1}$ yields

$$\mathbf{Y}_j^k = \sum_{l=0}^{L-1} h_l \mathbf{S}_j^k \mathbf{e}_{\tau_l} + \mathbf{V}_j^k = \mathbf{S}_j^k \mathbf{E}\mathbf{h} + \mathbf{V}_j^k \tag{3.5}$$

where the matrix $\mathbf{S}_j^k \in \mathbb{C}^{M\times M}$ is a diagonal matrix whose components are the frequency samples of $S_j^k(w)$ and the matrix $\mathbf{E} \in \mathbb{C}^{M\times L}$ contains the delay-signature vectors associated to each arriving delayed signal

$$\mathbf{E} = \begin{bmatrix} \mathbf{e}_{\tau_0} & \ldots & \mathbf{e}_{\tau_l} & \ldots & \mathbf{e}_{\tau_{L-1}} \end{bmatrix} \tag{3.6}$$

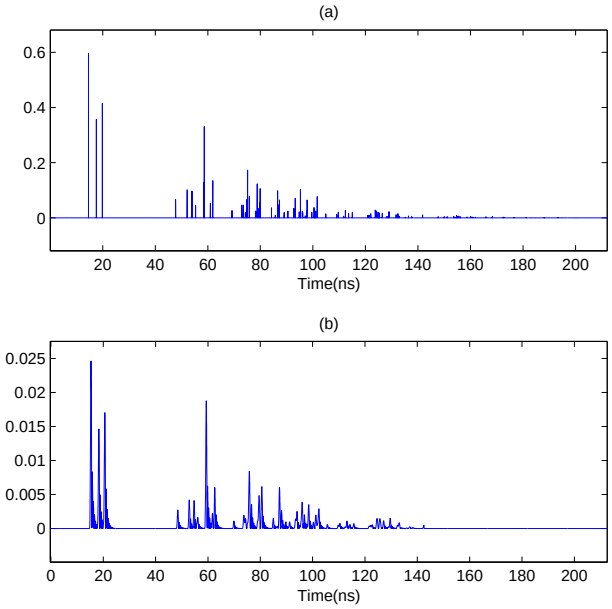

FIGURE 3.2: Signal through Channel: (a) Channel (b) Pulse propagated through the channel in (a)

with $\mathbf{e}_{\tau_l} = \begin{bmatrix} 1 & e^{-jw_0\tau_l} & \dots & e^{-jw_0(M-1)\tau_l} \end{bmatrix}^T$. The channel fading coefficients are arranged in the vector $\mathbf{h} = \begin{bmatrix} h_0 & \dots & h_{L-1} \end{bmatrix}^T \in \mathbb{R}^{L\times 1}$, and the noise samples in vector $\mathbf{V}_j^k \in \mathbb{C}^{M\times 1}$.

3.2 Sparse Frequency Domain Model

A proper sparse representation of the channel is required in order to easily apply the Compressed Sensing (CS) theory. A tutorial overview of some of the basic developments in CS can be found in [7]. The expression in (3.5) free of noise can be extended and reformulated as,

$$\mathbf{Y}_j^k = \mathbf{B}_j^k \mathbf{h}_e = \mathbf{S}_j^k \mathbf{E}_e \mathbf{h}_e \tag{3.7}$$

The main difference between (3.7) and (3.5) is the extended matrix $\mathbf{E}_e$, which is an $M \times M$ extended delay-matrix which contains not only the L delay-signature vectors corresponding to the multipath, but also $M-L$ delay-signature vectors with no channel contribution (see Fig. 3.3). Therefore, vector $\mathbf{h}_e$ is an *L-sparse* vector whose elements different from zero correspond to the original channel coefficients, that is, calling $\mathbf{e}_{\tau_m}$ the m-th column of $\mathbf{E}_e$, when

$$\mathbf{e}_{\tau_m} = \mathbf{e}_{\tau_l} \quad \text{for} \quad l = 0, \dots, L-1 \tag{3.8}$$

Note that the dimension M will determine the path resolution.

In a typical CS notation, $\mathbf{h}_e$ can be identified as the *L-sparse* vector and $\mathbf{B}_j^k \in \mathbb{C}^{M\times M}$ as the dictionary where the channel becomes sparse. In order to compress the frequency

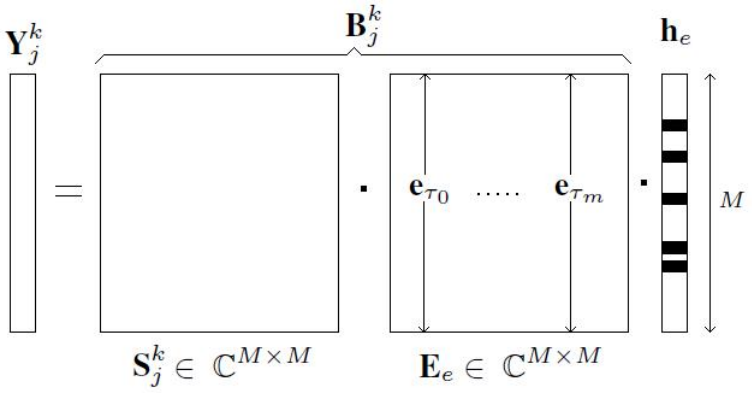

FIGURE 3.3: Sparse Sructure of the channel

domain samples a widely used random matrix $\mathbf{C}_f \in \mathbb{R}^{N\times M}$ with entries i.i.d. taken from a normal distribution with zero-mean and unit variance is used.

$$\mathbf{Y}_c = \mathbf{C}_f \mathbf{Y}_j^k = \mathbf{C}_f \mathbf{B}_j^k \mathbf{h}_e \tag{3.9}$$

where $\mathbf{Y}_c$ is the $N \times 1$ vector of measurements. $\mathbf{C}_f$ is known as measurement matrix and it has rank N lesser than the rank of the signal which is equal to M (see Fig. 3.4). Thus, the $N \times M$ matrix $\mathbf{C}_f$ is projecting the signal $\mathbf{Y}_j^k$. Randomness in the measurement matrix can lead to very efficient sensing mechanisms. It has been shown that random matrices are largely incoherent with any fixed basis (which is one of the principles of CS).

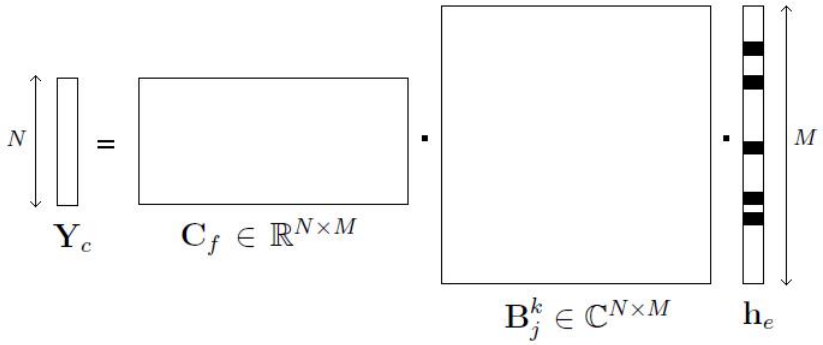

FIGURE 3.4: Compressed Sensing Structure

Therefore, the sparse channel estimation $\hat{\mathbf{h}}_e$ can be obtained from the compressed samples $\mathbf{Y}_c$ applying sparse signal reconstruction techniques. The sparse signal recovery problem is formulated as,

$$\min_{\hat{\mathbf{h}}_e \in \mathbb{R}^M} \left\| \hat{\mathbf{h}}_e \right\|_{l_1} \quad s.t. \quad \mathbf{Y}_c = \mathbf{C}_f \mathbf{B}_j^k \hat{\mathbf{h}}_e \tag{3.10}$$

where $\left\| \hat{\mathbf{h}}_e \right\|_{l_1} = \sum_{i=1}^{M} \left| \hat{h}_e(i) \right|$. Note that the only prior knowledge required is that $\mathbf{h}_e$ is sparse. Reconstruction then only requires the space in which the signal is sparse.

3.3 Sparse channel recovery

There are many approaches discussed in literature for solving (3.10). Besides from Section 2.1.4, a good reference to learn more about the algorithms for sparse signal recovery can be found in [18].

As it was said before, the sparsest solution can be obtained with l_0-norm optimization. Unfortunately, this optimization problem is unfeasible under computational point of view. The problem is relaxed using l_1-norm. Matching Pursuit (MP) [48] and Basis Pursuit (BP) [3] are the most popular approaches.

MP introduced by Mallat and Zhang is a pioneering work of greedy pursuit algorithms. With MP (and one of its variants OMP) the sparse signal is iteratively built up by selecting the atom that maximally improves the representation at each iteration. On the other hand, BP directly looks for the vector that minimize the l_1-norm coefficients, which is computationally expensive. In this thesis we will focus on OMP [8]-[53] because is the simpler, faster and more efficient solution.

3.3.1 MP variants: OMP

At each step of MP, the atom that has the strongest correlation with the residual signal is selected. This is what matching means. Note that MP selects atoms among the whole dictionary at each step. That means that an atom can be selected more than once, which slows down the convergence.

Orthogonal matching pursuit (OMP) [8] conquers this problem by projecting the signal onto the subspace spanned by the selected atoms. With this restriction OMP implies that no atom is selected twice. The resulting approximation is optimal in the least squares sense. Therefore, fewer steps are required to converge.

Based on the same key idea, Donoho et al. [54] proposed stagewise orthogonal matching pursuit (StOMP), with OMP as its special case. At each step, StOMP selects the atoms whose inner products with residue exceed a specially-designed threshold. Lower computational complexity is achived with StOMP compared with MP and OMP with similar sparsifying capability than BP.

Latter, Cotter and Rao [55] reduced the computation of atom matching by searching the atoms in a tree structure. The tree-structured searching was later fully studied by Jost et al. [56], known as tree-based pursuit (TBP). In a few words, TBP organize the dictionary in a tree structure: similar atoms are clustered together recursively until reaching a unique root. For each step, TBP selects the atom by traversing the tree from the root node until reaching a leaf node instead of searching over the whole dictionary. This is a simple way to develop fast searching algorithms.

In this thesis we will focuse on OMP algorithm because is simple, fast and provide good enough results.

3.3.2 OMP Historical Developments

OMP was developed independently by many researchers. A prototype of the OMP algorithm first appeared in the statistics community at some point in the 1950s, where

it was called stagewise regression. The algorithm later developed a life of its own in the signal processing [48] [53] [57] and approximation theory [58] [59] literatures. In this thesis it is used the adaptation for the signal recovery problem proposed in [8].

3.3.3 OMP Drawbacks

Of course not everything is good in OMP. Its simple and heurisic design lead to some drawbacks. It was demonstrated that if OMP selects a wrong atom in some iteration it might never recover the original signal. Skeptics pointed out that there is not solid theoretical foundation about its reliability. However, lots of studies have shown that it works in most of the cases and its widespread use in today's world are sufficient to believe in its reliability.

As it was commented before, OMP is computationally more demanding compared with MP but at the expense of ensuring that no repeated atoms are selected. Sometimes, the storage also becomes a problem, especially for highsized problems. Additionally, the OMP response against noise seems to be worse than other BP algorithms.

In my opinion, the most important drawback is the requirement of the level of sparsity to solve the problem. In our case of channel estimation we will never know the number of channels to be estimated a priori. Thus, in this master thesis we need a new criterion in order to decide when to halt the OMP algorithm and this design will have an important impact on the final performance of the algorithm. See section 3.3.5 for further information.

Despite the mentioned shortcomings, OMP is said to be the algorithm with better performance from the whole family of matching pursuits.

3.3.4 Extended OMP (eOMP)

Imperfections between the assumed model and the received signal can cause false path detection when using classic OMP. To improve the sparse signal recovery it is proposed an extended OMP (eOMP) (described with detail in Algorithm 1). Both OMP and eOMP are iterative greedy algorithms. The OMP select at each step the dictionary element best correlated with the residual part of the signal. Then it produces a new approximation by projecting the signal onto the dictionary elements that have already been selected. The main difference between OMP and eOMP is that eOMP not only pick the column of the dictionary that is most strongly correlated but also the $2k$ neighbors of it (see Fig. 3.5). Then, as OMP does, it produces a new approximation by projecting the signal onto the dictionary elements that have already been selected. To obtain the final values of the non-zero elements of the sparse vector in eOMP the same steps with only the most strongly correlated element is parallel computed.

The running time of the OMP is dominated by Step 2, whose total cost is $O(mNM)$ where m is the number of iterations. This step is the same for OMP and eOMP so the running time has not increased significantly due to the modifications introduced. In fact, the number of iterations m is reduced with eOMP due to the design itself. See next section for further information about the stopping criteria.

Algorithm 1 eOMP

Input

(·) An $N \times M$ matrix $\mathbf{C}_f\mathbf{B}_j^k$ which columns are expressed as φ_j

(·) An N dimensional data vector $\mathbf{Y}_c$

(·) An energy threshold

(·) Number of neighbors k (related to the pulse duration and the channel estimation resolution)

Procedure

(1) Initialize the residual $\mathbf{r}_0 = \mathbf{Y}_c$, the index sets $\Lambda_0 = \emptyset$ and $\Lambda_0^e = \emptyset$, and the iteration counter $t = 1$.

(2) Find the index λ_t that solves the easy optimization problem

$$\lambda_t = \arg \max_{j=1,\dots,N} |\langle \mathbf{r}_{t-1}, \varphi_j \rangle|$$

(3) Augment the extended and non-extended index set and the extended and non-extended matrix of chosen atoms:

$$\Lambda_t^e = \Lambda_{t-1}^e \cup \{\lambda_t - k\} \cup \ldots \cup \{\lambda_t\} \cup \ldots \cup \{\lambda_t + k\}$$

$$\Phi_t^e = \begin{bmatrix} \Phi_{t-1}^e & \varphi_{\lambda_t - k} & \cdots & \varphi_{\lambda_t} & \cdots & \varphi_{\lambda_t + k} \end{bmatrix}$$

$$\Lambda_t = \Lambda_{t-1} \cup \{\lambda_t\}$$

$$\Phi_t = \begin{bmatrix} \Phi_{t-1} & \varphi_{\lambda_t} \end{bmatrix}$$

We use the convention that Φ_0 and Φ_0^e are empty matrices.

(4) Solve the least square problem to obtain a new signal estimate

$$\mathbf{x}_t^e = \arg \min_{\mathbf{x}} \|\mathbf{Y}_c - \Phi_t^e \mathbf{x}\|_2^2$$

$$\mathbf{x}_t = \arg \min_{\mathbf{x}} \|\mathbf{Y}_c - \Phi_t \mathbf{x}\|_2^2$$

(5) Calculate the new approximation of the data and the new residual

$$\mathbf{a}_t = \Phi_t^e \mathbf{x}_t^e$$

$$\mathbf{r}_t = \mathbf{Y}_c - \mathbf{a}_t$$

(6) Increment t, and return to Step 2 if the energy threshold is not achieved.

(7) The estimate $\hat{\mathbf{h}}_e$ for the ideal signal has nonzero indices at the components listed in Λ_t and the value of the estimate $\hat{\mathbf{h}}_e$ in component λ_j equals the j-th component of $\mathbf{x}_t$.

$$\hat{\mathbf{h}}_e(\Lambda_t) = \mathbf{x}_t$$

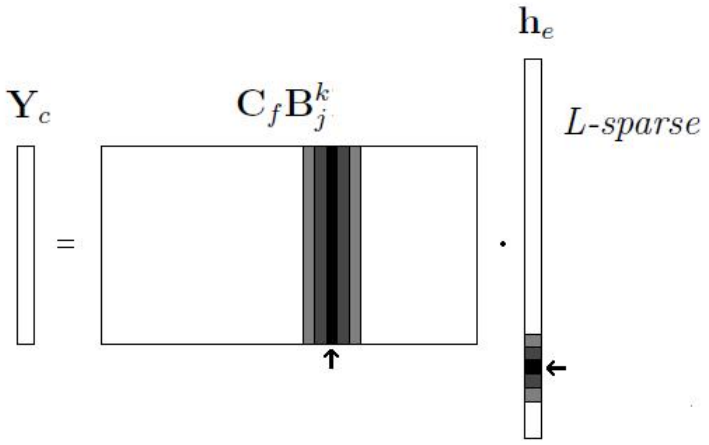

FIGURE 3.5: eOMP not only pick the column of the dictionary that is most strongly correlated but also the $2k$ neighbors

Therefore, it is clear that the idea behind the algorithm is to pick columns in a greedy fashion. At each iteration we look for the column of $\mathbf{C}_f\mathbf{B}_j^k$ that is most strongly correlated with the remaining part of $\mathbf{Y}_c$.

3.3.5 eOMP Stopping Criteria

The sparsity level is assumed to be known in the classical version of OMP. As it was mentioned before, in the sparse channel estimation problem the number of paths to be estimated is not known a priori. Thus, in our case, after each iteration, the algorithm has to decide whether or not to proceed. It may just stop after a fixed number of iterations, or it may use current information more subtly to determine whether another iteration would be beneficial.

Algorithms for the estimation of channels whose impulse reponse is sparse involving OMP are well studied in the literature. Since OMP is an iterative algorithm, in general they all face the same problem: a method for deciding when to halt the iteration.

Previously reported approaches [60] [61] try to determine when a channel tap is active (non-zero) based on the use of a measure requiring the definition of an *activity* threshold. Such measures are chosen according to some intuitive criterion. Other approaches try to limit the reconstruction error obtained under some threshold. As Joel A. Tropp comment in [62], there are several natural methods for deciding when to halt the iteration. He summarizes all the methods in the following classification:

- Halt the algorithm after a fixed number of iterations.
- Halt the algorithm when $\|\mathbf{r}_t\|_2$, the norm of the residual, declines below a specific tolerance.
- Halt the algorithm when $\left\|\left(\mathbf{C}_f\mathbf{B}_j^k\right)^H \mathbf{r}_t\right\|_\infty$, the maximum correlation between the residual and the dictionary, drops below some threshold.

Naturally, the appropiate criterion depends on the application domain. Next it is indicated which criterion is chosen for the problem we are facing.

As it was introduced when describing the eOMP algorithm, here we will use a stopping criteria based on the noise energy level. However, in order to simplify the simulations, the energy threshold mentioned in Section 3.3.4 is computed as a function of the received signal free of noise energy and the received signal energy, both without compressing,

$$E_{th}(\%) = \frac{E_{r_{wn}}}{E_r} \times 100 \tag{3.11}$$

with $\mathbf{r}_{wn}$ being the received signal without noise. In general, $\mathbf{r}_{wn}$ is not available to the receiver and therefore the percentage $E_{th}(\%)$ has to be computed based on the estimated noise energy level.

Therefore, the algorithm is halted when the energy of $\mathbf{C}_f\mathbf{B}_j^k\hat{\mathbf{h}}_e^t$ achieve the corresponding percentage of $\mathbf{Y}_c$. Here we have use the notation $\hat{\mathbf{h}}_e^t$ to denote the sparse channel estimation at the end of the iteration t, which is formed as $\hat{\mathbf{h}}_e^t(\Lambda_t) = \mathbf{x}_t$.

The mean energy threshold used in simulations is plotted in Fig. 3.6. Remember that this threshold is the percentage of signal without noise over the noisy signal. It can be observed that starting at SNR=10dB the energy threshold begin to fall down below the 90%. It has to be mentioned that we are taking advantage of the inherent temporal diversity of the IR-UWB signal, with N_f repeated transmitted pulses for each information symbol by averaging over all the available symbols.

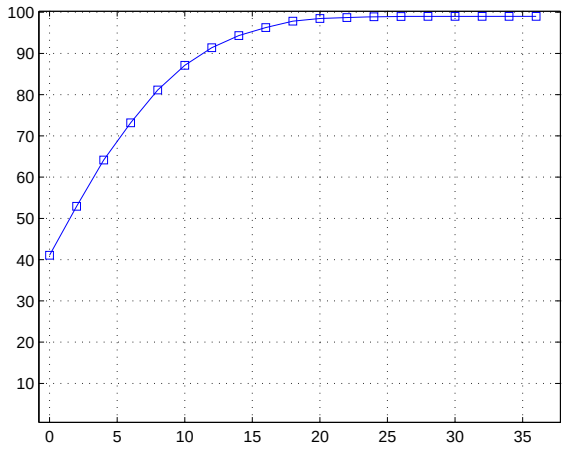

FIGURE 3.6: Threshold Energy

4
Simulations

For numerical evaluation of the algorithm we consider the channel models developed within the framework of the IEEE 802.15.4a. In particular it is used the CM1 Residential LOS channel model [50]. All simulations are given for 100 independent channel realizations. M is fixed at 768 and the compression rate is expressed with $\rho = \frac{N}{M}$.

The compression rate notation has been extracted from [63]. ρ measures the degree of determinacy/indeterminacy of the system: $0 < \rho < 1$, with $\rho = 1$ meaning the matrix $\mathbf{C}_f\mathbf{B}_j^k$ is square and so the system $\mathbf{Y}_c = \mathbf{C}_f\mathbf{B}_j^k\mathbf{h}_e$ is well determinated, while $\rho << 1$ meaning the matrix $\mathbf{C}_f\mathbf{B}_j^k$ is very wide and the system $\mathbf{Y}_c = \mathbf{C}_f\mathbf{B}_j^k\mathbf{h}_e$ is very undeterminated. Equivalently, ρ is the undersampling factor: $\rho = 1$ indicates marginal undersampling while $\rho << 1$ means high undersampling.

The pulse duration is equal to 0.77ns (which theoreticaly correspond to a compression rate equal to $\rho = 0.333$ if we want to acquire the same samples than an ADC working at the Nyquist rate). The number of multipath components L that form the UWB channel can be quite large, however many of those paths are negligible. Therefore, we limit ourselves to estimate the L_c most significant paths which are the ones capturing 80% of the channel energy.

The algorithm input signal is obtained taking advantage of the inherent temporal diversity of the UWB signal, with N_f repeated transmitted pulses for each information symbol. This approach provides robustness to noise compared to applying the estimator individually to each arriving frame.

The quality of the channel estimation is evaluated with the RMSE computed as,

$$RMSE = \frac{1}{M}\mathbf{e}^H\mathbf{e} \tag{4.1}$$

where the error $\mathbf{e}$ is defined as,

$$\mathbf{e} = \mathbf{ifft}(\mathbf{B}_j^k\hat{\mathbf{h}}_e) - \mathbf{r}_{wn} \tag{4.2}$$

with $\mathbf{r}_{wn}$ being the received signal without noise.

4.1 Receiver Structure

Imagine a receiver that picks up the analog received signal and directly applies an AIC converter. We will assume that the analog signal can be interpreted as a digital signal with a lot of samples (that tend to infinity). Look at Fig. 4.1 where a scheme is proposed only to clarify the concept. After the compression step, the signal is passed though the OMP algorithm in order to obtain the sparse channel estimation.

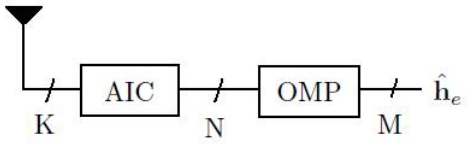

FIGURE 4.1: Receiver Scheme

The approach proposed in this thesis assumes finite-dimensional model for the analog signal like general problems treated in the context of CS. Prof. Yonina Eldar from the Israel Institute of Technology has developed and is still working on a few on-going research projects regarding the analog compressed sensing. Her contribution is a methodology for sub-Nyquist sampling, named Xampling. A summary of her work related to the analog compressed sensing can be found in [64] and [65]. A large collection of the vastly growing reserach literature on the subject is available on Yonina's webpage: **http://webee.technion.ac.il/Sites/People/YoninaEldar**

The details of the compressed sensing implementation are considered as out of the scope of this thesis and the discussion is limited to the theoretical evaluation of the proposed model and the performance of the new proposed algorithm. Nevertheless, implementation of CS systems is a hot topic on the CS research world and, in some cases, a very thin implementation has been realized.

4.2 Why eOMP?

4.2.1 OMP Weakness

Let us begin with a simple example. Imagine the channel depicted in Fig. 4.2 and the resulting signal when the mother pulse propagates through this particular channel (also depicted in Fig. 4.2).

To see the insights of the OMP procedure, here the compression is not applied in order to plot the inverse Fourier Transform of the OMP output. Therefore the model considered *in this example* is,

$$\mathbf{Y}_c = \mathbf{Y}_j^k = \mathbf{B}_j^k \mathbf{h}_e \tag{4.3}$$

where $\mathbf{B}_j^k \in \mathbb{C}^{M \times M}$ is the dictionary where the channel becomes sparse and $\mathbf{Y}_c$ is the $M \times 1$ vector of measurements. There is no compression.

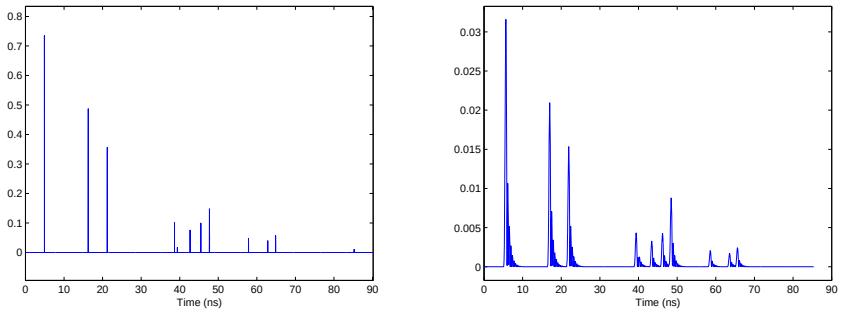

(a) Channel (b) Received signal

FIGURE 4.2: A channel realization and its corresponding received signal

The inputs of the OMP algorithm are: $\mathbf{Y}_c$, $\mathbf{B}_j^k$ and the energy threshold. In the absence of noise, the OMP is stopped when the recovered signal achieves 99% of the input compressed signal. In our particular example it corresponds to 12 iterations.

In the first iteration, the first channel active tap is set at 4.8889ns. However the first path in the channel is at 4.91ns. This mismatch is due to the limited resolution of the sparse estimated channel, which can never achieve the analog resolution. Fig. 4.3 shows the original received pulse compared with the reconstructed pulse with the resulting estimated channel after the first iteration. The differences are hard to see but they exist and that would be a problem for us.

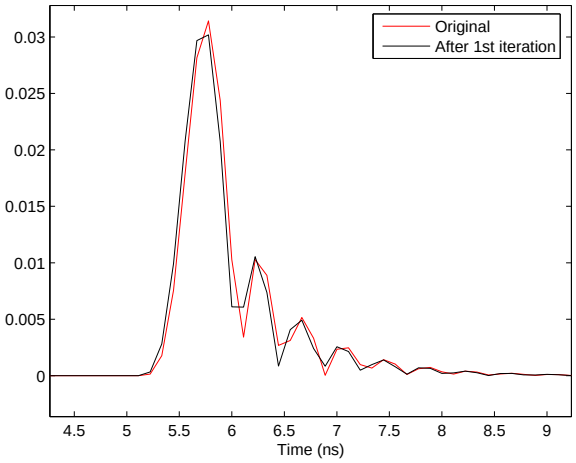

FIGURE 4.3: Original received pulse compared with the reconstructed one using the sparse channel estimation after first iteration

In Fig. 4.4 the input signal $\mathbf{Y}_c$ is plotted in (a) and the remaining part of $\mathbf{Y}_c$ after extracting the contribution of the first selected atom of the dictionary is plotted in (b). It can be observed how the contribution of the first path is not completely removed.

This remaining part of pulse will cause the appearance of a false path at iteration number 8. The algorithm assume that this residual contribution is caused by another

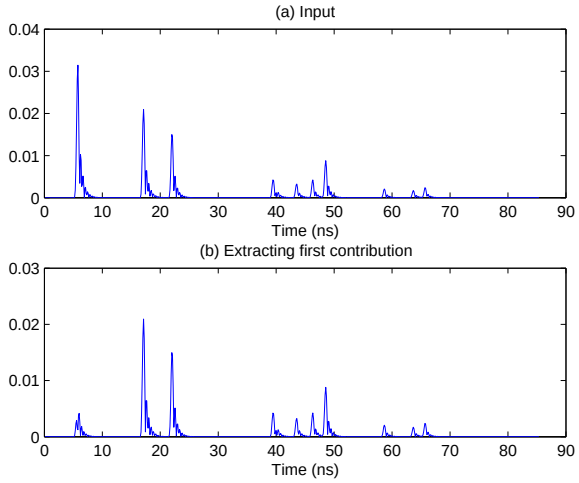

FIGURE 4.4: Comparison within the original input $\mathbf{Y}_c$ and the remaining part of it after extracting the contribution of the first selected atom of the dictionary

path and tries to substract it. In Fig. 4.5, the input $\mathbf{Y}_c$, the residual signal at iteration number 7 and the residual signal at iteration number 8 are plotted in (a),(b) and (c) respectively. A zoom has been made at the area of interest in Fig. 4.6 where it can be better perceived the difference between (b) and (c).

Finally, in Fig. 4.7 is depicted the real channel compared with the sparse channel estimation obtained with the OMP algorithm. With black arrows are pointed out the false path introduced by OMP due to the imperfections between the model and the real received signal. These errors will persist and probably increase when compressing the signal. Finally in Fig. 4.7 is also depicted the sparse channel estimation applying a compression with $\mathbf{C}_f \in \mathbb{R}^{N \times M}$. It can be seen that the false path detected are higher than before.

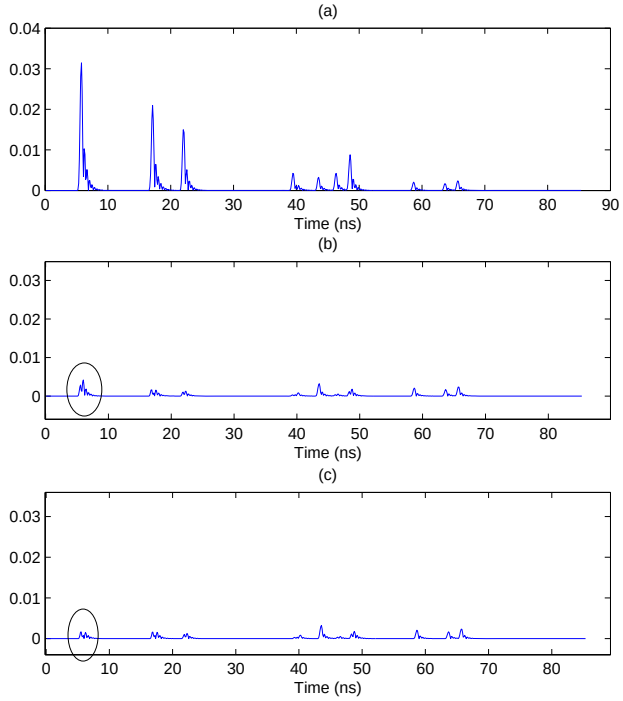

FIGURE 4.5: Residual Signal (1): (a) Original $\mathbf{Y}_c$ (b) Residual signal at iteration number 7 (c) Residual signal at iteration number 8

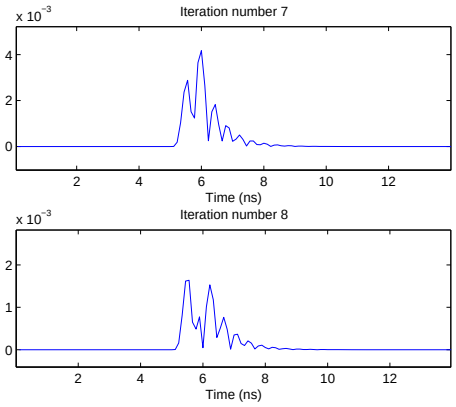

FIGURE 4.6: Received Residual Signal (2): Zoom of Fig. 4.5 at the area of interest

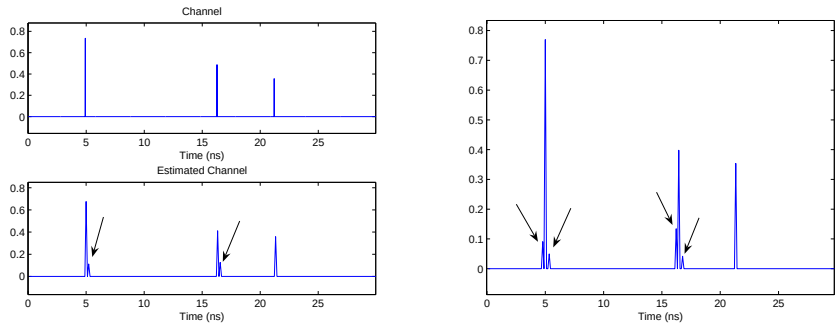

(a) Resulting sparse channel estimation compared with the real channel

(b) Resulting sparse channel estimation compressing with $\mathbf{C}_f \in \mathbb{R}^{N \times M}$

FIGURE 4.7: Resulting sparse channel estimation

4.2.2 OMP improvement: eOMP

The goal of the extended OMP is to remove the false path detection. The main difference between OMP and eOMP is that eOMP not only pick the column of the dictionary that is most strongly correlated but also the $2k + 1$ neighbors. Proceeding in this way ensures that the contribution of that particular path is completely removed. Therefore, the eOMP tends to *clean* the channel estimation obtained by classic OMP. A critical parameter is k: if k is chosen so high it could happen that the algorithm miss some real important paths (low detection probability) and if k is chosen so low it could still happen high false path detection probability. We will show simulations varying the parameter k later.

Now, focusing on the comparison between OMP and eOMP, let's see a simple example as before. Look at Fig. 4.8 where is plotted a particular channel realization compared with the channel estimation obtained with OMP and eOMP. With black arrows are indicated the false path detected and with black circles are indicated the missed paths. The recovered signal RMSE computed is equal to 0.0016659 for the eOMP and 0.0017609 for the OMP. Regarding the TOA estimation, it is easy to see that with eOMP it is simple to detect the TOA of the first detected path. With eOMP, the TOA estimation error is 0.078788 meters while using eOMP it is equal to 0.0016659 meters.

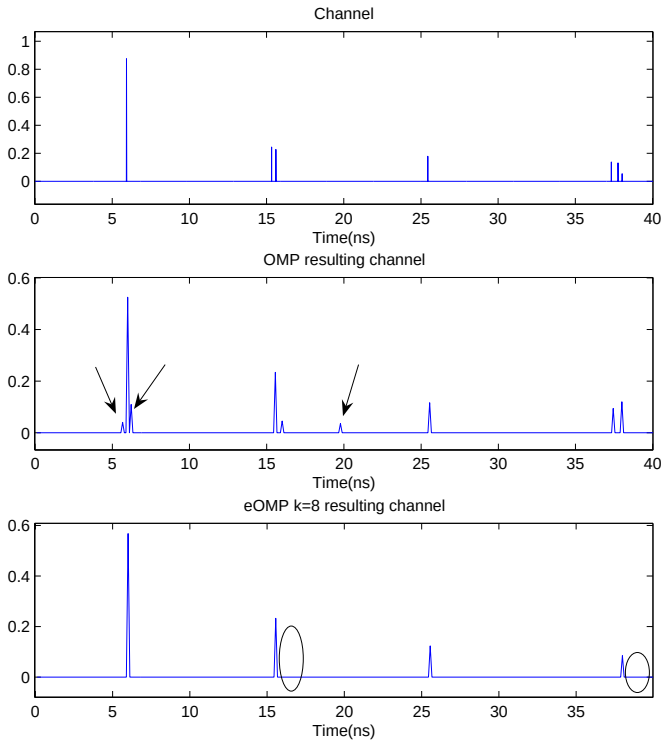

FIGURE 4.8: Comparison between OMP and eOMP for a particular channel realization

It is important to highlight that if eOMP doesn't miss any path, the recovered signal with eOMP outperforms the recovered signal with OMP since OMP is assuming false paths. Unfortunately, to ensure that we are not missing any path is not an easy task. Nevertheless, the TOA estimation is expected to improve using eOMP. All these hypotheses strongly depend on the parameter k chosen.

If k is low, it means that we are not missing so many paths but we can still have false path detection. The TOA could be wrong if the first detected pulse still have some false path close to him. On the other hand, if k is high we are ensuring that we make no false detections at the expense of a low correct path detection probability.

The criterion for choosing the value of k would depend on the final objective of each application.

4.3 eOMP vs OMP

A comparison with the classical OMP will be developed in order to show the performance of the proposed eOMP.

First and foremost, the RMSE of the reconstructed signal is evaluated. Fig. 4.9 depicts the RMSE of the reconstructed signal using OMP and eOMP for different compression rates. Examining the reconstruction error of each algorithm as a function of the SNR, we observe that OMP exhibits slightly better performance than eOMP. However, the biggest diference is of the order of 10^{-4} and it decreses as the noise level increases. Although OMP obtains lots of false path detections (we will see this in Fig. 4.11), they have low contribution to the overall channel. Thus, the contribution of the false paths detected by OMP affect less on the reconstruction than missing paths with big contribution. That is what is happening when using eOMP whatever the value of k: we have no false path detection but probably we are missing some paths with significant contribution to the overall channel. It is also confirmed by the fact that the error increases ad the value of k increases, meaning that the higher the value of k, the more the missing paths. The previous hypothesis will be checked with other simulation results. Regarding to the compression rate, it can be observed that the error increase as the compression rate decrease whatever the algorithm is used. Thus, the recovery performance improves as we take more measurements.

To show that the classical OMP provides better correct path detection let us now study the probability of detecting a true path of OMP compared with the proposed eOMP. Fig. 4.10 provides the simulation results regarding the correct path detection probability using OMP and eOMP for different compression rates. Prior to the simulations we have commented that a high value on the parameter k could cause miss detection of true paths. This is the reason why in Fig. 4.10 we have obtained higher correct path detection when k is equal 2. The fact that OMP is detecting more true paths than eOMP is also proved with these results. Thus, OMP always exhibits more correct path detection than eOMP in part because the more paths detected, the more likely hitting a true one. Regarding to the compression rate, it can be observed that the probability of correct path detection decrease as the compression rate decrease whatever the algorithm is used.

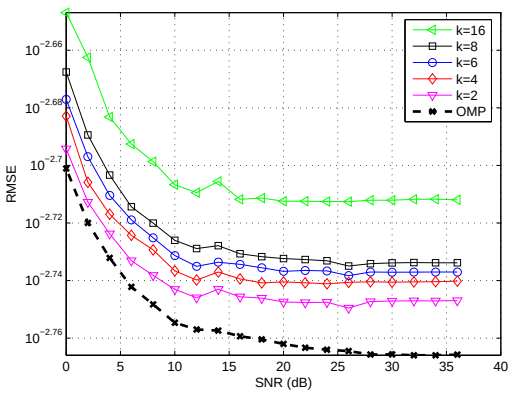

(a) $\rho = 0.333$

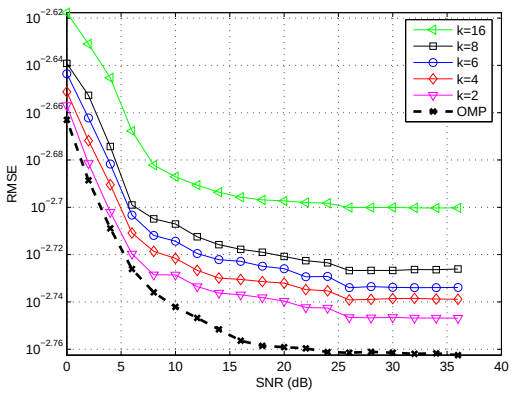

(b) $\rho = 0.167$

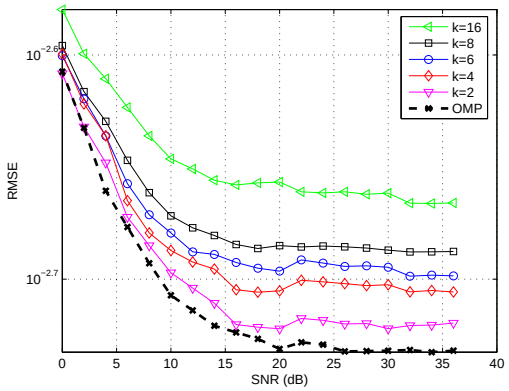

(c) $\rho = 0.083$

FIGURE 4.9: RMSE of the recovered signal. Comparison between OMP and eOMP for different compression rates.

With Fig. 4.10 we show that the correct path detection probability is sensitive to the compression rate. It can be observed that $\rho = 0.083$ leads to perceivable performance loss compared with the curves corresponding to $\rho = 0.333$ and $\rho = 0.167$. From the comparison of the three compression rates is concluded that the more the samples acquired, the better the correct path detection probability.

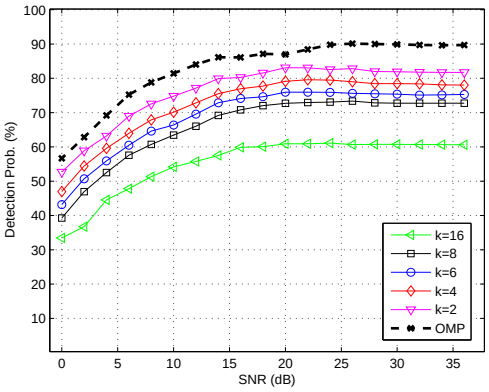

(a) $\rho = 0.333$

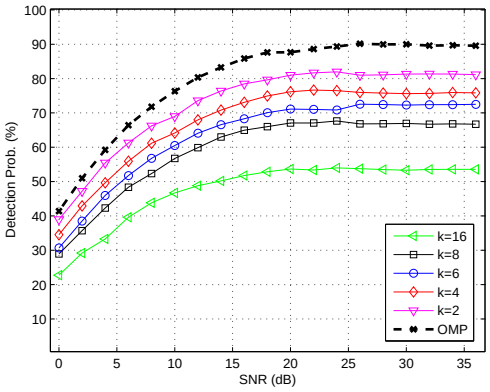

(b) $\rho = 0.167$

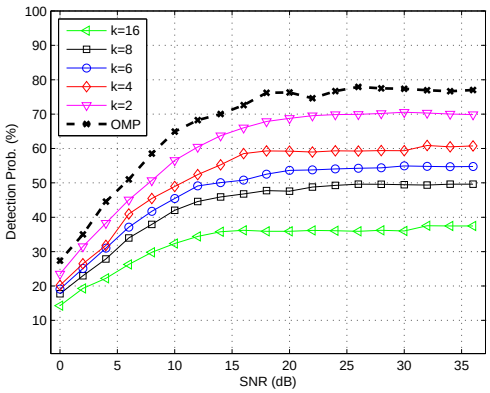

(c) $\rho = 0.083$

FIGURE 4.10: Correct path detection probability. Comparison between OMP and eOMP for different compression rates.

Again, to confirm that the proposed eOMP reduces the false path detection let us now study the probability of false path detection of eOMP compared with the classical OMP. Fig. 4.11 depicts the false path detection probability using OMP and eOMP for different compression rates. The results show that the false path detection probability is significantly reduced when using eOMP. For the same reason as before, a high value on the parameter k could cause, in addition to miss detection of true paths, low false path detection probability.

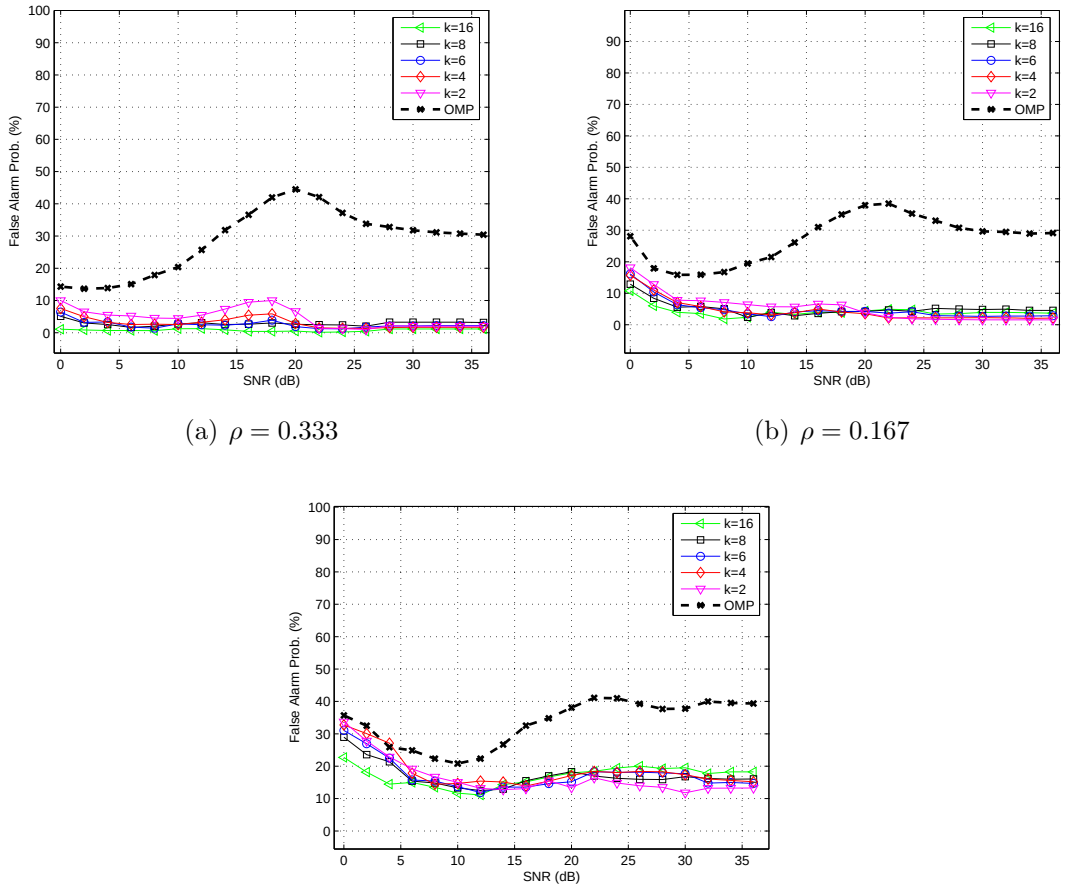

(a) $\rho = 0.333$

(b) $\rho = 0.167$

(c) $\rho = 0.083$

FIGURE 4.11: False path detection probability. Comparison between OMP and eOMP for different compression rates.

One thing that attracts our attention is the peak of false alarms around the 20dB of SNR. The peak can be perfectly seen in the case of OMP and, although not distinguish very well, it persists in the case eOMP. To understand what is happening, Fig. 4.12 shows the number of iterations required for OMP and eOMP for different compression rates.

The first conclusion extracted from Fig. 4.12 is that another advantage of eOMP compared with classical OMP is its high speed. In eOMP fewer steps are required to converge. This is a direct consequence of the eOMP design itself. The stopping

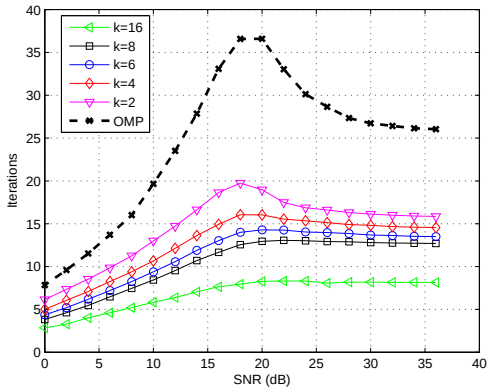

(a) $\rho = 0.333$

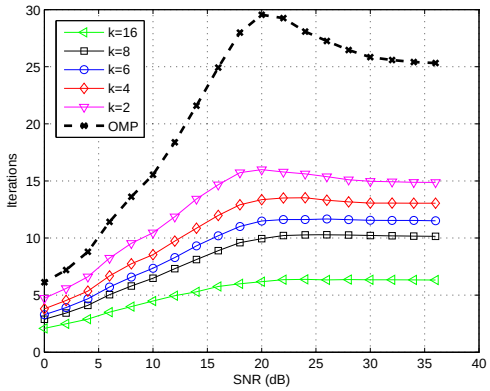

(b) $\rho = 0.167$

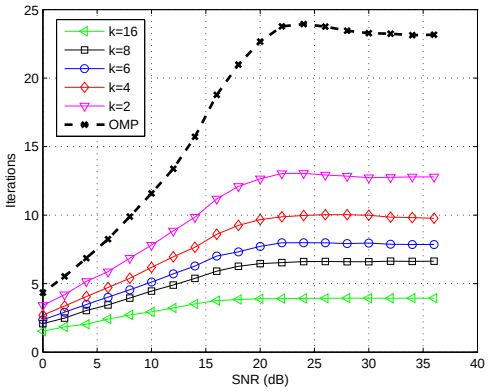

(c) $\rho = 0.083$

FIGURE 4.12: Number of Iterations. Comparison between OMP and eOMP for different compression rates.

criteria is a function of the number of neighbors used since the recovered signal energy is computed using all the neighbors. Returning to the peak of false alarms observed in Fig. 4.11, we can see that the iterations also have a peak at the same point of SNR=20dB. This demonstrates that it is possible that we are running the algorithm too long, when, in fact, we should stop the algorithm much earlier. As it was commented in Section 3.3.5, the design of a convenient method for deciding when to halt the iteration is a difficult task. A natural stopping rule for the subset selection problem is not immediately apparent. Here an intuitive stopping criteria is being used but, apparently it is a point for further research.

Besides the peak, the number of iterations remain constant whatever the compression rate is.

The RMSE of the estimated TOA using OMP and eOMP are depicted in Fig. 4.13 for different compression rates

The general conclusion about the TOA estimation is that eOMP achieve better TOA estimation than OMP. In particular, whatever the value of k the behavior for

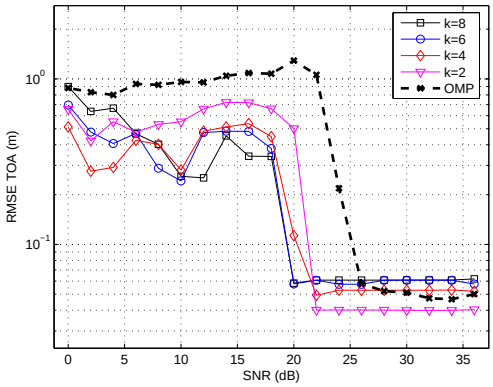

(a) $\rho = 0.333$

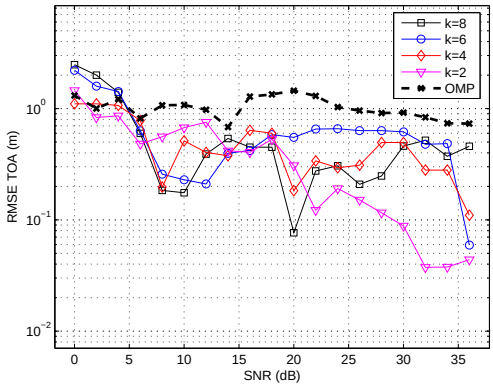

(b) $\rho = 0.167$

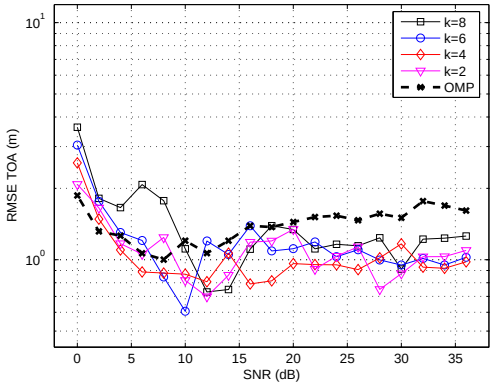

(c) $\rho = 0.083$

FIGURE 4.13: RMSE of the estimated TOA. Comparison between OMP and eOMP for different compression rates.

high SNR is similar in both cases, achieving an accuracy of 5 cm when $\rho = 0.333$ (this is when there is no compression, the number of mesurements is the same for an ADC working at the Nyquist rate). In general, the behavior of eOMP is more o less the same whatever the value of k.

The improvement provided by eOMP is still present when the compression rate is set at $\rho = 0.167$ (this corresponds to the half the measurements acquired by an ADC at Nyquist rate). In this case, the simulation results show that with eOMP k=2 an accuracy of few centimeters is achieved while the OMP accuracy is about one meter. Therefore, is clearly seen how the eOMP algorithm outperforms the classical OMP. Unfortunately, using a compression rate equal to the fourth part of samples acquired by an ADC working at the Nyquist rate (this is $\rho = 0.083$), the differences are not so obvious but still significant.

4.4 Time Domain vs Frequency Domain

The perfomance of the new frequency domain estimator is compared with the time domain sparse model proposed in [1].

In [1], Jose L. Paredes et Al. wonder if a new dictionary that better fits the UWB model can be generated in order to better represent the sparseness of the signal. Inspecting the characteristic of the received UWB waveform, which is formed by scaled and delayed versions of the transmitted pulse, they naturally derive a new dictionary based on the pulse waveform used to covey the information. This leads to a set of parametrized waveforms given by,

$$d_j(t) = p(t - j\Delta) \tag{4.4}$$

that define the dictionary $D = \{d_0(t), d_1(t), d_2(t), ..., \}$ where Δ is a shifting parameter. The idea is simple: use a dictionary with delayed versions of the UWB mother pulse.

Therefore, the dictionary used here for simulations is a circulant matrix $\mathbf{P} \in \mathbb{R}^{M \times M}$ whose columns are shifted replicas of the mother pulse $p(t)$. The compressed samples are obtained with a random measurement matrix as in (3.9),

$$\mathbf{y}_c = \mathbf{C}_t \mathbf{P} \hat{\mathbf{h}}_e \tag{4.5}$$

where $\mathbf{C}_t \in \mathbb{R}^{N \times M}$. In this case the RMSE is obtained with the following error definition,

$$\mathbf{e} = \mathbf{P}\hat{\mathbf{h}}_e - \mathbf{r}_{wn} \tag{4.6}$$

For a complete study we have compared [1] with the new sparse model proposed here considering: OMP, eOMP k=2, eOMP k=4, eOMP k=6, eOMP k=8 and eOMP k=16.

4.4.1 OMP

In Fig. 4.14 the RMSE of the reconstructed signal, the false path detection probability, the correct path detection probability and the number of iterations required using the model proposed in [1] and the number of iterations required, all obtained using OMP for both the time domain approach proposed in [1] and the frequency domain approach proposed here. The results are compared for different compression rates.

The simulation results shown that the new frequency domain sparse model outperforms the time domain sparse model proposed in [1] when using OMP. Whatever the algorithm used and whatever the value of k, the new model achieve better results regarding the recovery process. At the compression rate $\rho = 0.333$ (equivalent to an ADC working at the Nyquist rate), the RMSE remains more or less the same for both approaches. However, as the compression rate decrease, the errors in the time domain increase faster than the frequency domain errors.

The better performance achieved with the frequency domain sparse model with respect to the time domain sparse model can be justified from a theoretical point of view using the incoherence property. As it was explained in Section 2.1.3, the incoherence is defined as the maximum value amongst inner product of the dictionary and the

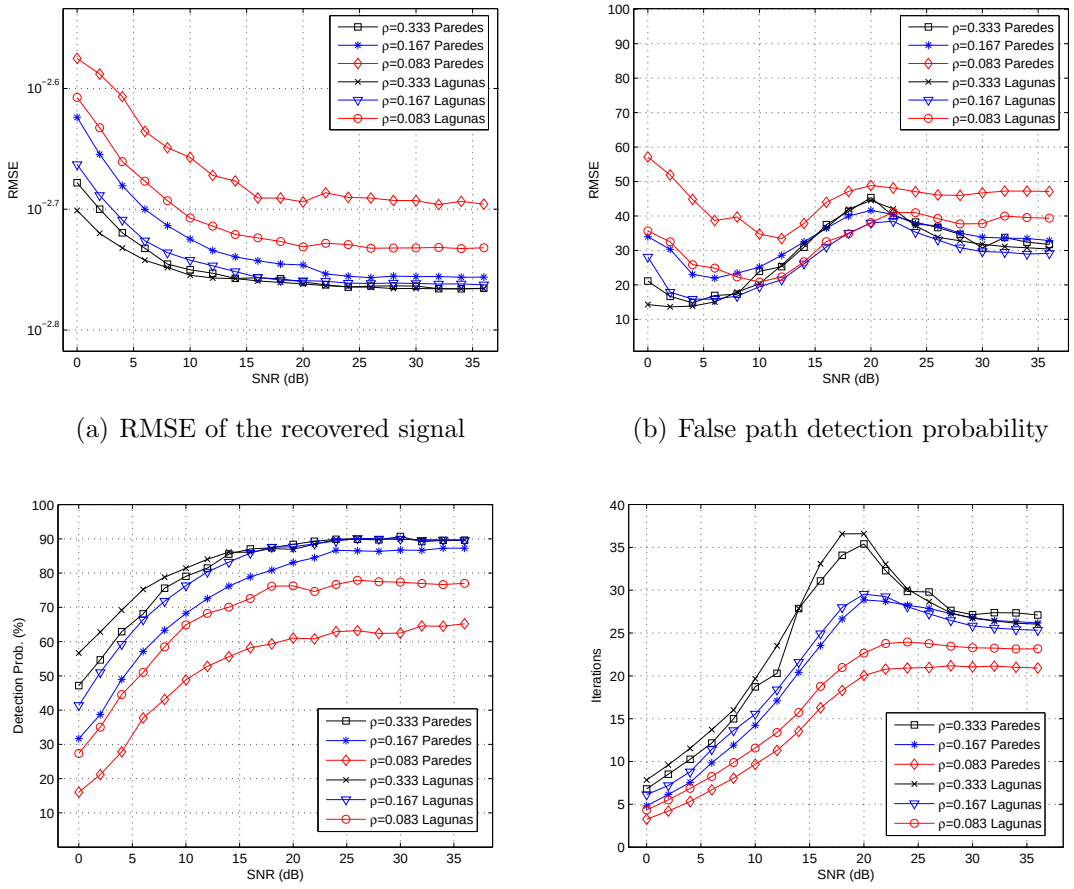

(a) RMSE of the recovered signal

(b) False path detection probability

(c) Correct path detection probability

(d) Number of Iterations

FIGURE 4.14: Comparison between the proposed model and [1] using OMP

orthonormal measurement matrix. A low value of incoherence is desirable in order to ensure mutually independent matrices and therefore better compressive sampling. The spike basis achieves maximal incoherence with the Fourier basis and is for that reason that seems more convenient to work with frequency domain measurements. Although here the dictionary $\mathbf{P}$ is not the identity matrix and the dictionary $\mathbf{SE}$ is not the Fourier matrix, they both are approximations of these.

The same happens with the false path detection probability. The time doamin approach proposed in [1] tend to exhibit higher false path detection than the frquency domain sparse model proposed in this thesis, especially when the compression rate decreases.

For the correct path detection probability, the same conclusion as for the false path detection probability is extracted. The new frequency domain sparse model outperforms the model proposed in [1]. Again the differences increase as the compression rate decrease.

Regarding the number of iterations, the algorithm requires more or less the same number of iterations for both sparse models.

Fig. 4.15 depicts the RMSE of the estimated TOA using OMP for [1] and for the frequency domain approach proposed here.

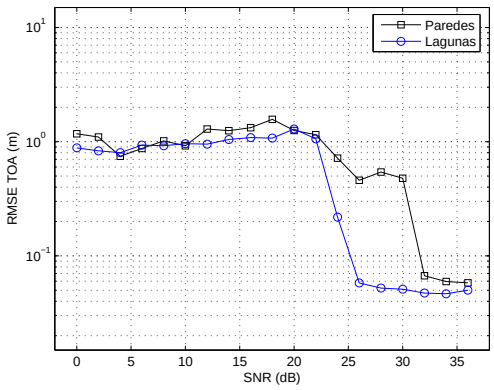

(a) $\rho = 0.333$

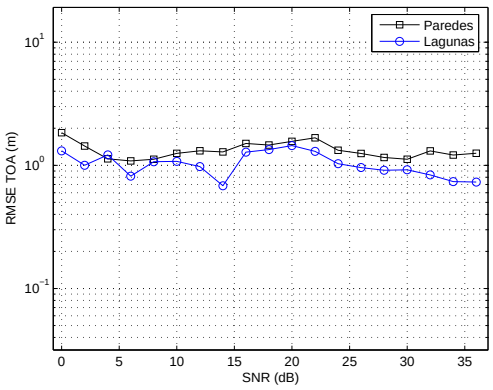

(b) $\rho = 0.167$

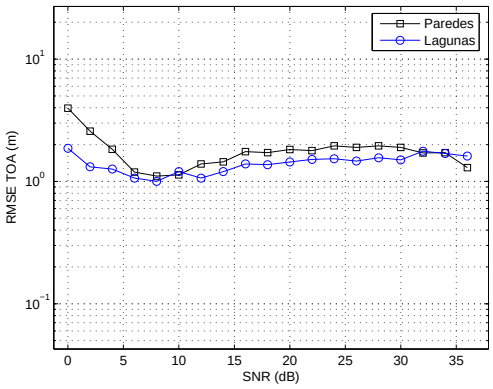

(c) $\rho = 0.083$

FIGURE 4.15: RMSE of the estimated TOA. Comparison with [1] using OMP

Simulation results show that the new frequency domain sparse model slightly outperforms the time domain sparse model proposed in [1] regarding the TOA estimation. The curve corresponding to the RMSE of the estimated TOA corresponding to the new frequency domain sparse model is always below the curve corresponding to [1].

4.4.2 eOMP

A comparison between [1] and the new sparse model proposed here has been done considering the new eOMP for different number of neighbors.

First of all, in Fig. 4.16 is shown the RMSE of the reconstructed signal for different values ok k. As happened before, the curve corresponding to the new frequency sparse model always achieves better reconstruction error than the model proposed in [1]. The differences increase as the compression rate decreases.

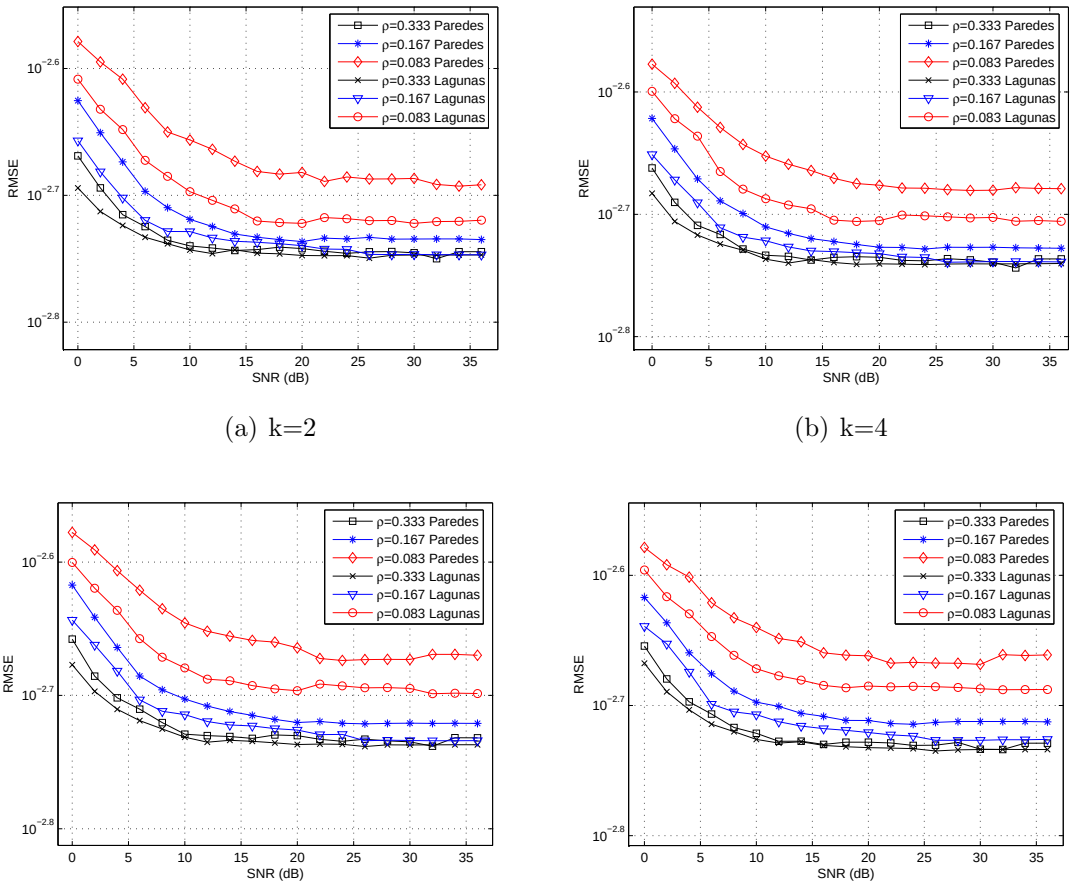

(a) k=2 (b) k=4

(c) k=6 (d) k=8

FIGURE 4.16: RMSE of the recovered signal. Comparison between the proposed model and [1] using eOMP

Fig. 4.17 compares the correct path detection probability using eOMP for [1] and the frequency domain approach followed here. From the simulation results we can conclude that using the new model, the correct path detection is improved, specially when the compresion rate decreases.

Fig. 4.18 depicts the false path detection probability corresponding to the model proposed in [1] and the false path detection probability obtained assuming the new frequency sparse model proposed here, both using eOMP. We observe that [1] works

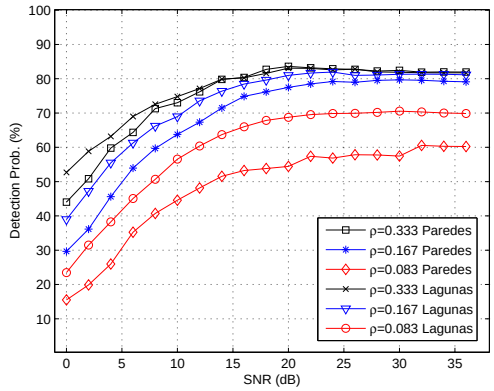

(a) k=2

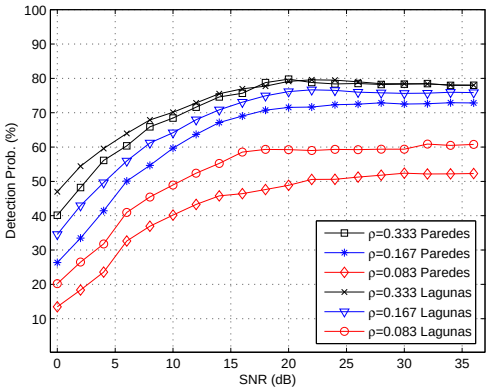

(b) k=4

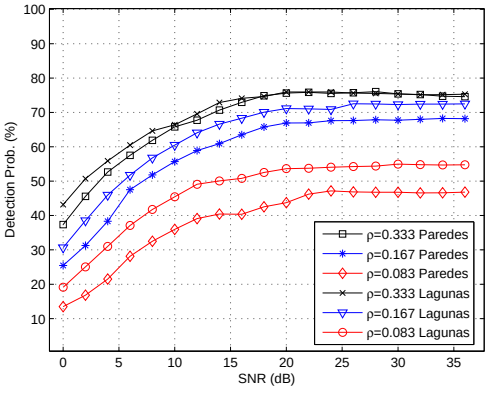

(c) k=6

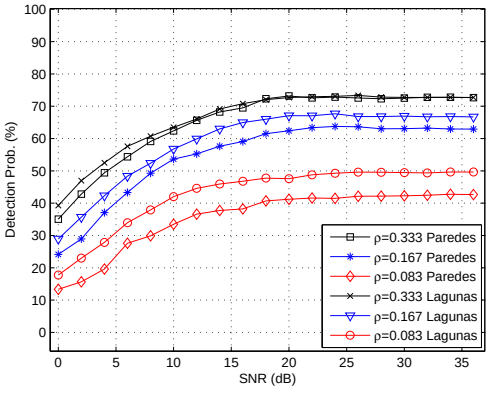

(d) k=8

FIGURE 4.17: Correct path detection probability. Comparison between the proposed model and [1] using eOMP

slightly worse than the new model regarding the false path detection probability, whatever the compresion rate is.

In Fig. 4.19 are shown the number of iterations required using [1] and using the frequency domain approach proposed here, both using eOMP. There are no significant differences between [1] and the new model regarding to the running time of the algorithm. Both approaches take the same number of iterations to achieve the final result.

To show the TOA estimation performance, the simulation results are divided into different figures (each figure corresponding to a different value of k) in order to easily draw the conclusions. Fig. 4.20, Fig. 4.21, Fig. 4.22 and Fig. 4.23 depict the RMSE of the estimated TOA using eOMP for [1] and for the frequency domain approach proposed here for k equal to 2,4,6 and 8, respectively.

Simulation results show that the frequency domain sparse model proposed here significantly outperfomes the time domain sparse model proposed in [1] regarding the

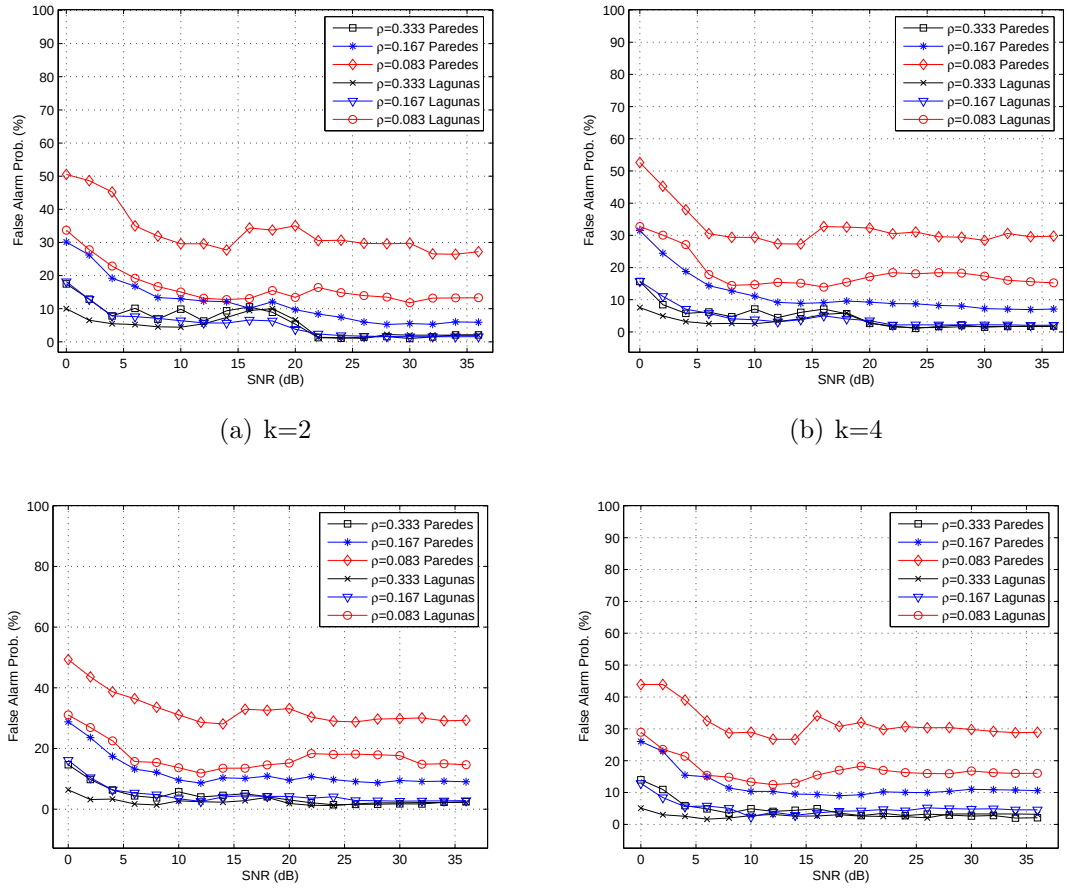

(a) k=2 (b) k=4

(c) k=6 (d) k=8

FIGURE 4.18: False path detection probability. Comparison between the proposed model and [1] using eOMP

TOA estimation. The curve corresponding to the RMSE of the estimated TOA corresponding to the frequency domain approach goes always below the curve corresponding to [1]. Moreover, the TOA estimation accuracy of [1] is always above half meter.

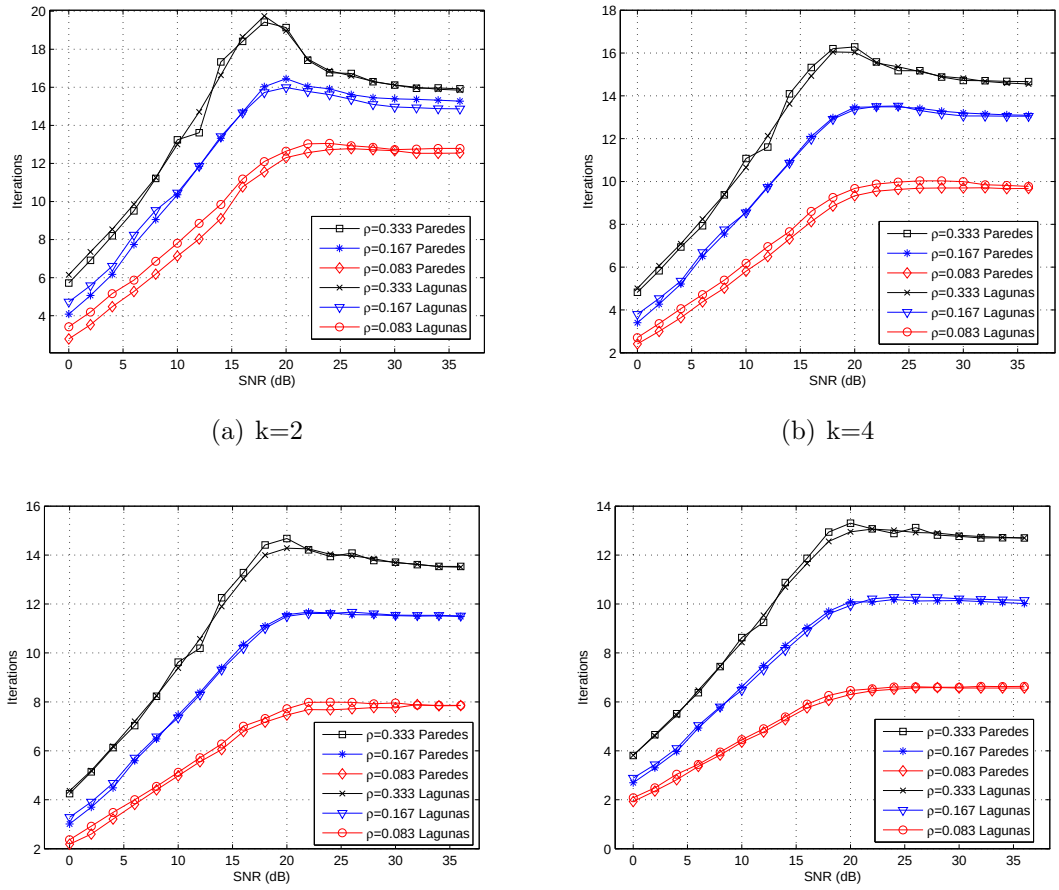

(a) k=2 (b) k=4

(c) k=6 (d) k=8

FIGURE 4.19: Number of Iterations. Comparison between the proposed model and [1] using eOMP

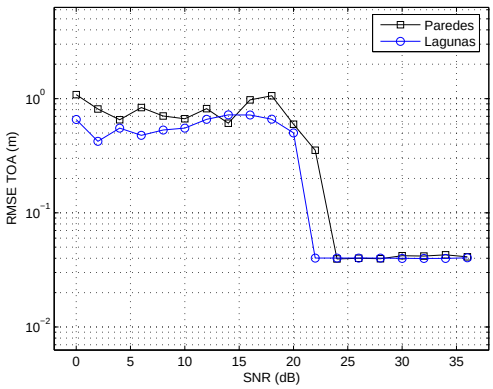

(a) $\rho = 0.333$

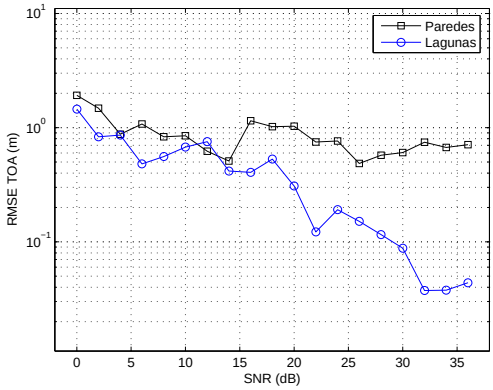

(b) $\rho = 0.167$

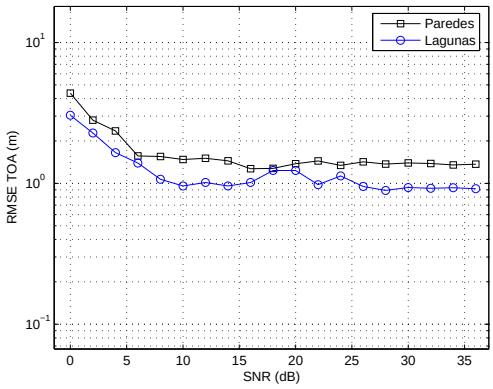

(c) $\rho = 0.083$

FIGURE 4.20: RMSE of the estimated TOA. Comparison with [1] using eOMP (k=2)

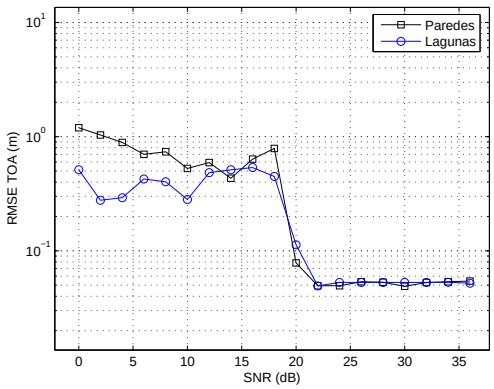

(a) $\rho = 0.333$

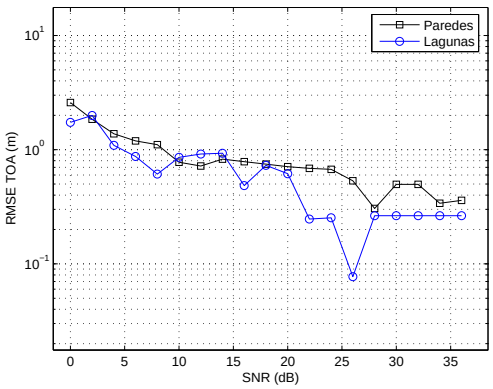

(b) $\rho = 0.167$

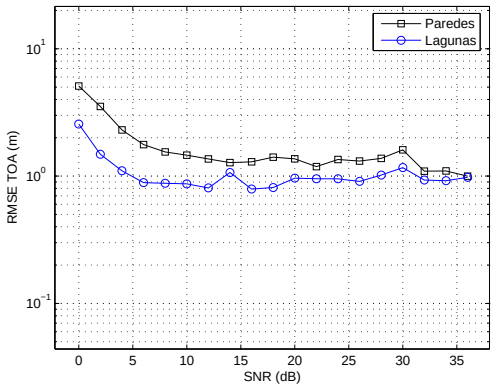

(c) $\rho = 0.083$

FIGURE 4.21: RMSE of the estimated TOA. Comparison with [1] using eOMP (k=4)

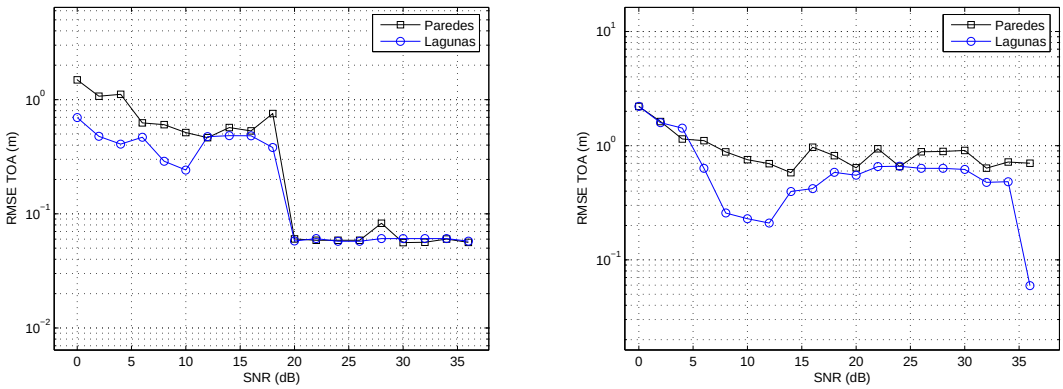

(a) $\rho = 0.333$ (b) $\rho = 0.167$

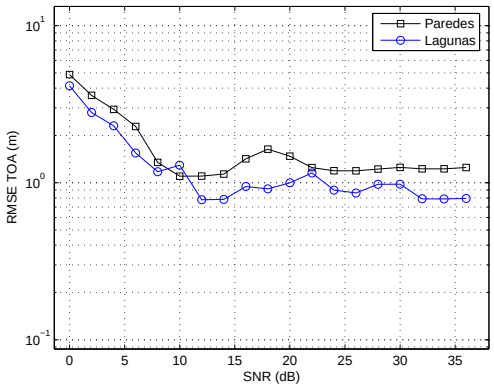

(c) $\rho = 0.083$

FIGURE 4.22: RMSE of the estimated TOA. Comparison with [1] using eOMP (k=6)

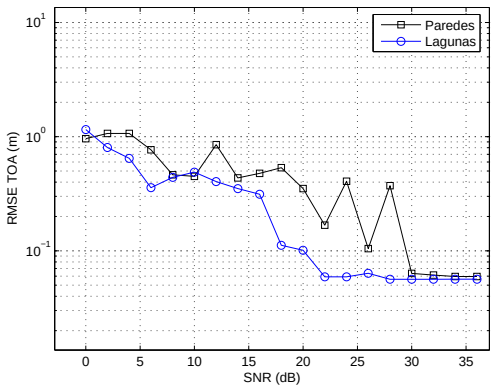

(a) $\rho = 0.333$

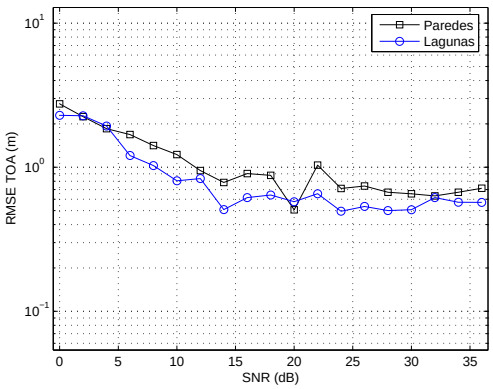

(b) $\rho = 0.167$

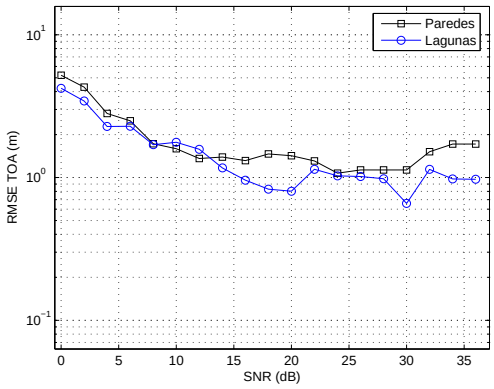

(c) $\rho = 0.083$

FIGURE 4.23: RMSE of the estimated TOA. Comparison with [1] using eOMP (k=8)

4.5 Naini vs new model

A comparison with another frequency domain model presented in [2] has been done. In [2], the spectrum is spread pre-modulating the input signal with a pseudorandom sequence $p[n]$ before the Fourier transformation ensuring that every measurement carries information,

$$\mathbf{y}_c = \mathbf{RF}\text{diag}(p[n])\mathbf{Ph}_e \tag{4.7}$$

where $\mathbf{F}$ is the column normalized DFT matrix and $\mathbf{R}$ is the sub-sampling operator (an N by M matrix filled with zeroes except one element on each row that is equal to M/N and such that there is at most one non-zero element on each column). Therefore $\mathbf{RF}$ is simply standard Fourier sub-sampling matrix.

As before, for a complete study we have compared [2] with the new sparse model proposed here considering: OMP, eOMP k=2, eOMP k=4, eOMP k=6, eOMP k=8 and eOMP k=16.

4.5.1 OMP

Fig. 4.24 compares the RMSE of the reconstructed signal, the false path detection probability, the correct path detection probability and the number of iterations required obtained with OMP for the frequency domain approach proposed in [2] and the frequency domain approach proposed here. The results are compared for different compression rates.

The simulation results shown that the new frequency domain sparse model outperforms the one proposed in [2] if we consider the classical OMP. At the Nyquist compression rate (meaning $\rho = 0.333$), the RMSE remains more or less the same for both approaches. However, as the compression rate decreases, the errors using [2] increase faster than the error using the new sparse approach.

The same conclusion can be derived for the false path detection probability. The new frequency domain sparse model outperforms the model proposed in [2] regarding the correct path detection probability. Again the differences increase as the compression rate decrease.

The number of iterations required are more or less the same for both sparse models.

Fig. 4.25 depicts the RMSE of the estimated TOA using OMP for [2] and for the frequency domain approach proposed here.

Simulation results show that the frequency domain sparse model proposed here significantly outperforms the time domain sparse model proposed in [2] regarding the TOA estimation. The curve corresponding to the RMSE of the estimated TOA corresponding to the frequency domain sparse model proposed here goes always below the curve corresponding to [2].

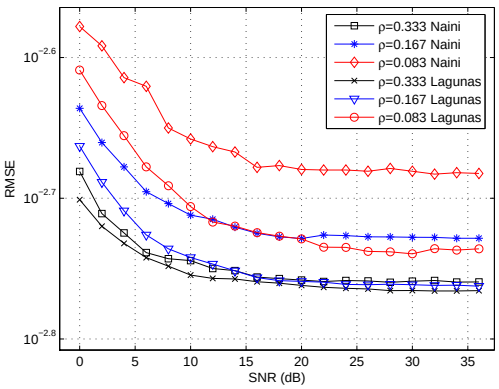

(a) RMSE of the recovered signal

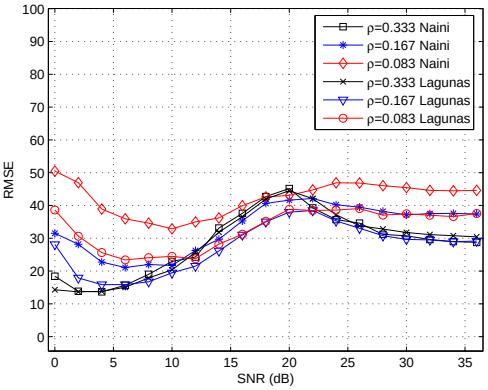

(b) False path detection probability

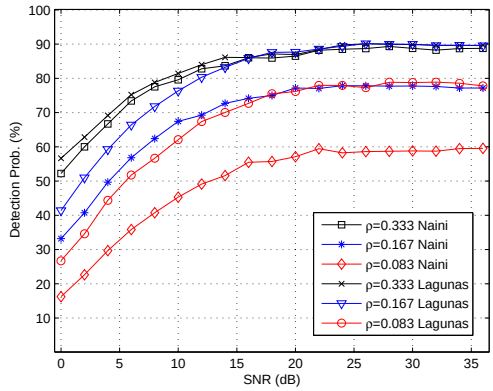

(c) Correct path detection probability

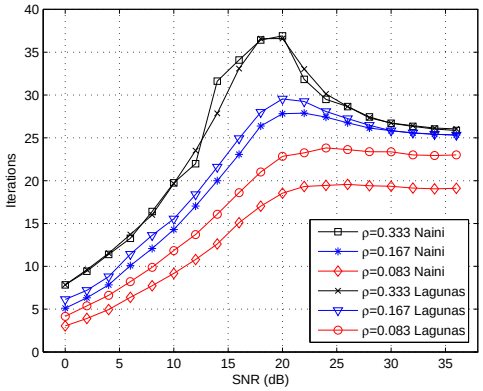

(d) Number of Iterations

FIGURE 4.24: Comparison between the proposed model and [2] using OMP

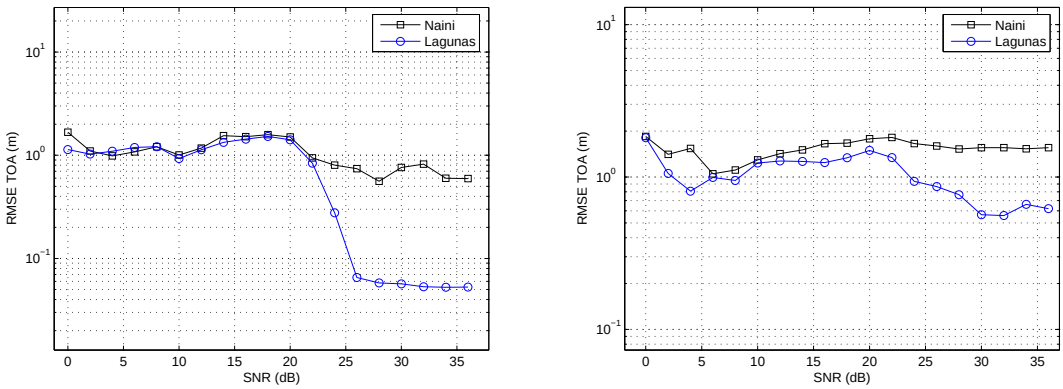

(a) $\rho = 0.333$ (b) $\rho = 0.167$

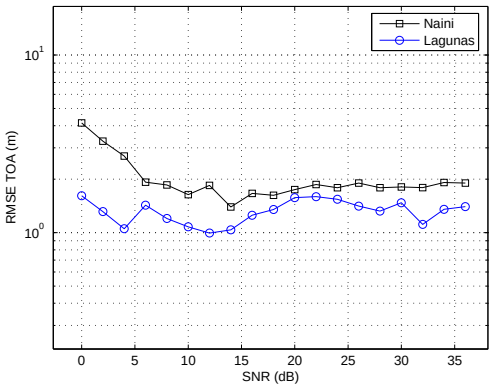

(c) $\rho = 0.083$

FIGURE 4.25: RMSE of the estimated TOA. Comparison with [2] using OMP

4.5.2 eOMP

Fig. 4.26 compares the RMSE of the reconstructed signal obtained with eOMP for the frequency domain approach proposed in [2] and for the frequency domain approach proposed here. The results are compared for different compression rates.

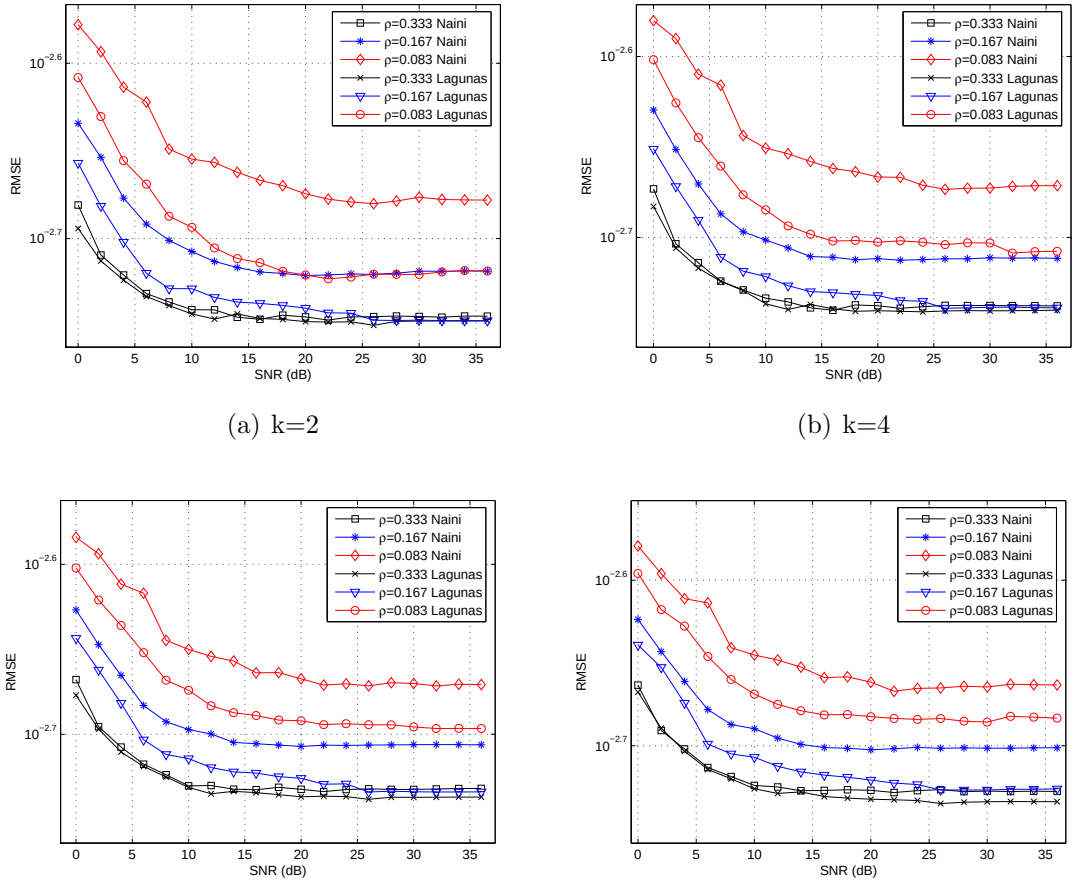

(a) k=2 (b) k=4

(c) k=6 (d) k=8

FIGURE 4.26: RMSE of the recovered signal. Comparison between the proposed model and [2] using eOMP

At first sight, it can be conclude that the frequency model proposed here improves the reconstruction error provided by [2], at least when the compression rate is reduced. The improvements are not only illustrated in the reconstruction process, but also in Fig. 4.27 and Fig. 4.28 where the corresct path detection and the false path detection probabilities are shown, respectively. In both, the frequency domain sparse model proposed here outperforms the one proposed in [2], providing higher probability of correct path detection and lower probability of false path detection. Again the differences increase as the compression rate decrease.

Fig. 4.29 shows that there are no differences on the running time of the algorithms depending on the model used.

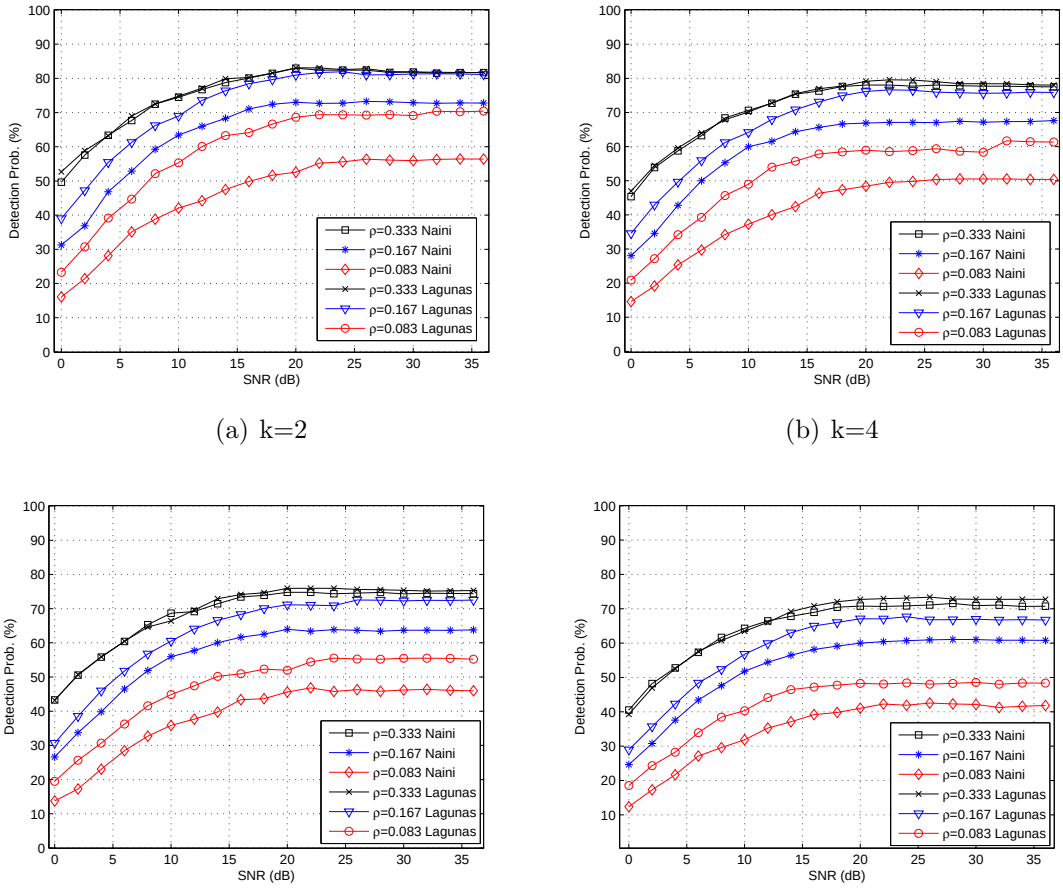

(a) k=2 (b) k=4

(c) k=6 (d) k=8

FIGURE 4.27: Correct path detection probability. Comparison between the proposed model and [2] using eOMP

To show the TOA estimation performance, as before the simulation results are divided into different figures (each figure corresponding to a different value of k) in order to easily draw the conclusions. Fig. 4.30, Fig. 4.31, Fig. 4.32 and Fig. 4.33 depict the RMSE of the estimated TOA using eOMP for [2] and for the frequency domain approach proposed here for k equal to 2,4,6 and 8, respectively.

Whatever the value of k, the TOA estimation error obtained with [2] is higher than the error obtained with the frequency sparse model proposed in this thesis. The differences are enlarged when the compresion rate increases.

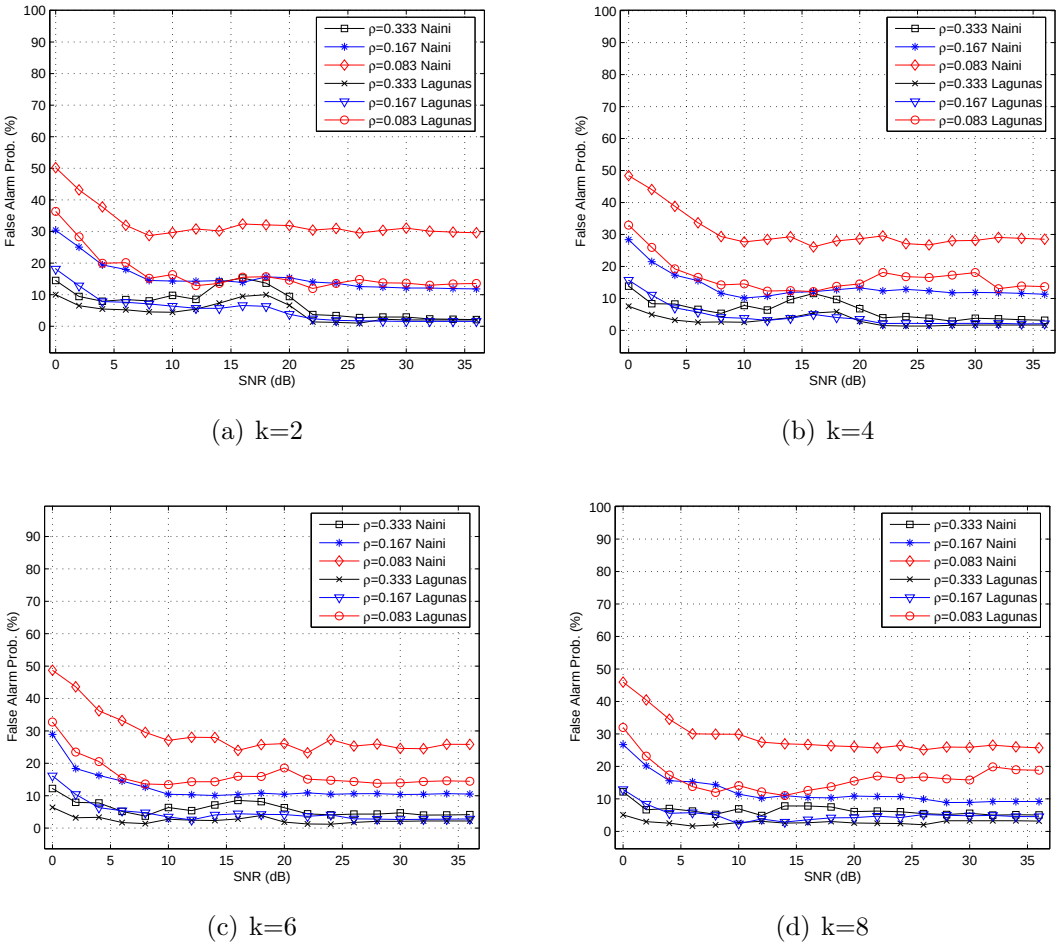

(a) k=2 (b) k=4

(c) k=6 (d) k=8

FIGURE 4.28: False path detection probability. Comparison between the proposed model and [2] using eOMP

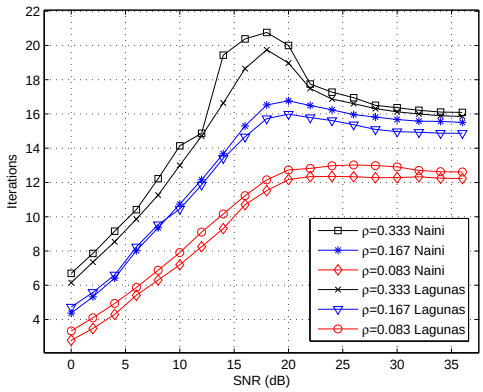

(a) k=2

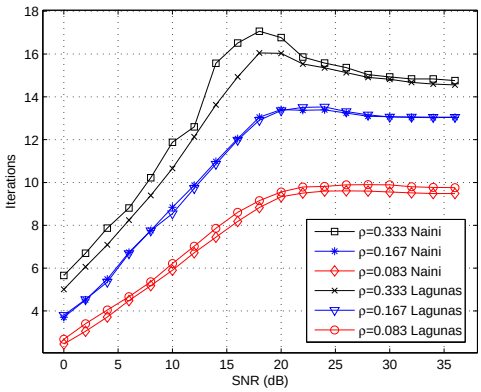

(b) k=4

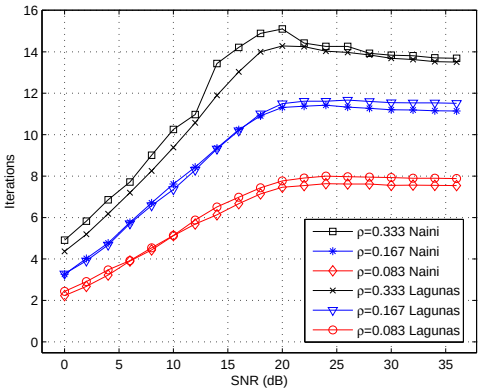

(c) k=6

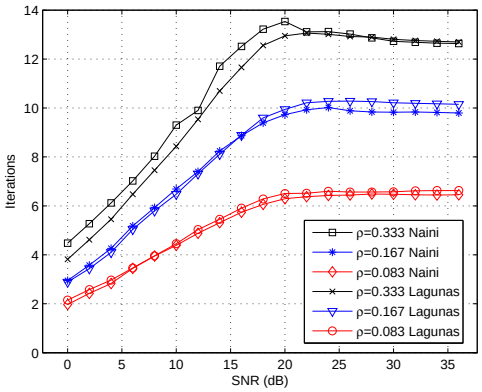

(d) k=8

FIGURE 4.29: Number of Iterations. Comparison between the proposed model and [2] using eOMP

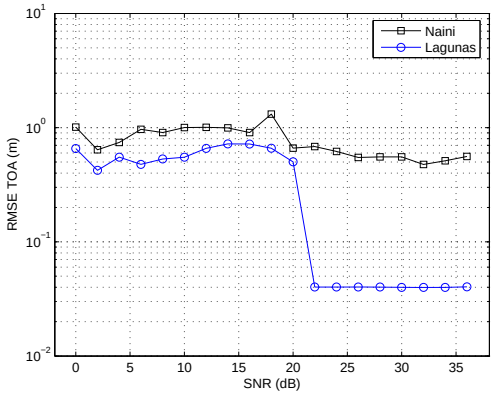

(a) $\rho = 0.333$

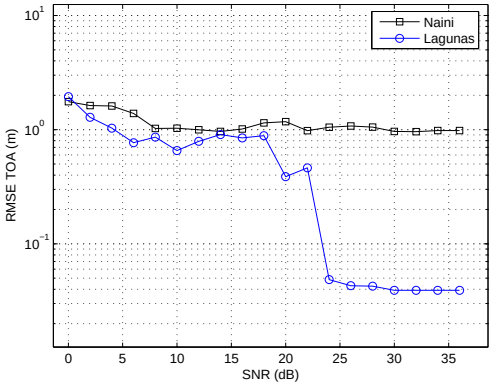

(b) $\rho = 0.167$

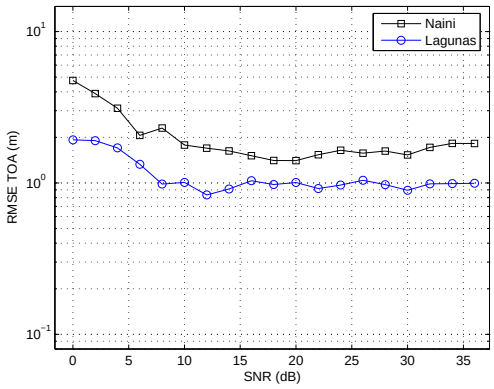

(c) $\rho = 0.083$

FIGURE 4.30: RMSE of the estimated TOA. Comparison with [2] using eOMP (k=2)

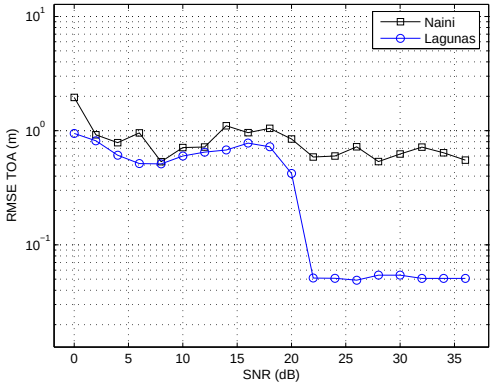

(a) $\rho = 0.333$

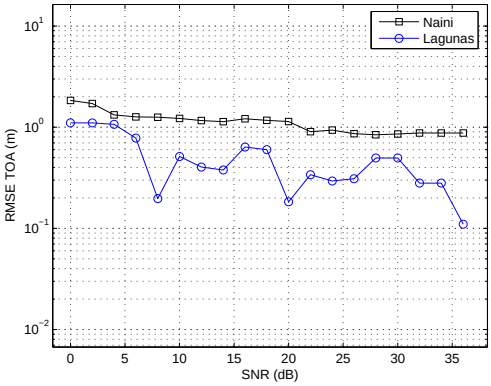

(b) $\rho = 0.167$

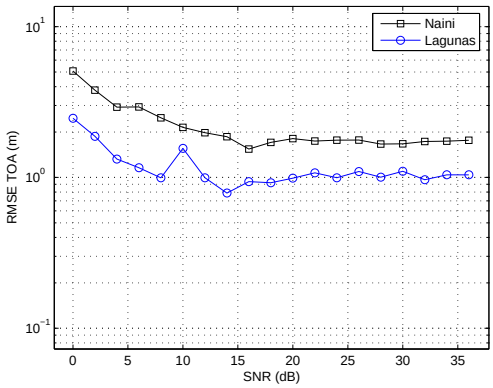

(c) $\rho = 0.083$

FIGURE 4.31: RMSE of the estimated TOA. Comparison with [2] using eOMP (k=4)

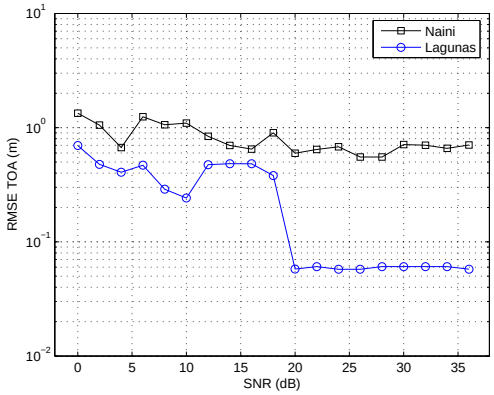

(a) $\rho = 0.333$

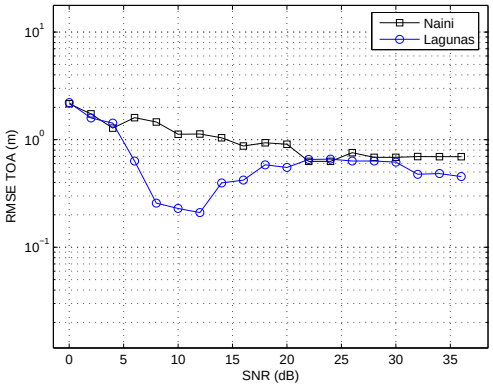

(b) $\rho = 0.167$

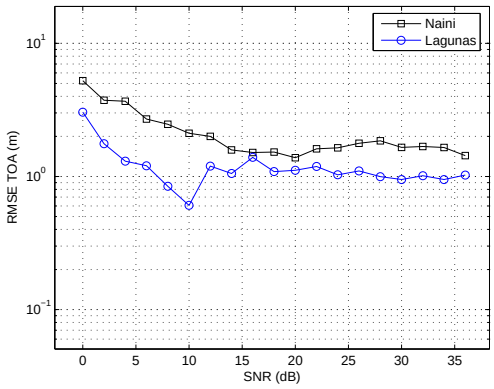

(c) $\rho = 0.083$

FIGURE 4.32: RMSE of the estimated TOA. Comparison with [2] using eOMP (k=6)

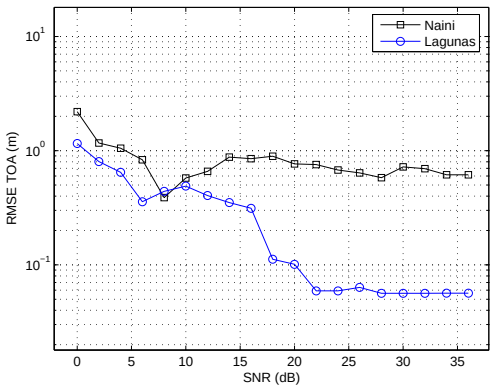

(a) $\rho = 0.333$

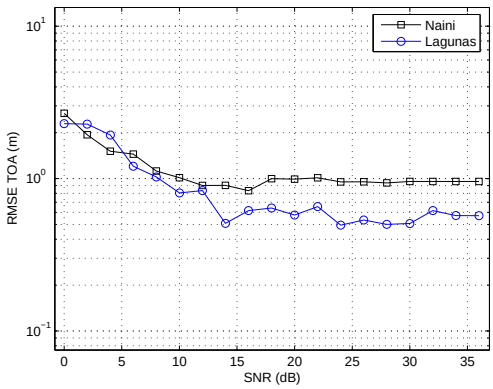

(b) $\rho = 0.167$

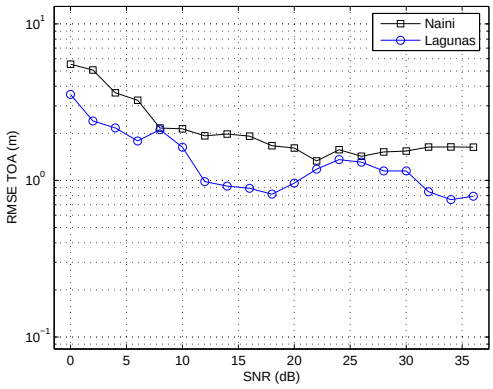

(c) $\rho = 0.083$

FIGURE 4.33: RMSE of the estimated TOA. Comparison with [2] using eOMP (k=4)

4.6 Summary

A frequency domain UWB sparse channel estimator based on the compressed sensing (CS) theory has been presented. The identified shortcomings of the classical OMP leaves a gap which here is filled with a new algorithm called extended OMP (eOMP).

Therefore, a new algorithm named eOMP based on the classic OMP is proposed in order to improve some OMP characteristics. It has been shown that the new eOMP provides lower false path detection probability compared with classical OMP, which also leads to a better TOA estimation, without significant degradation of the channel estimation.

Simulation results of the new sparse channel estimator are compared with a time domain approach presented in [1] and with another frequency model presented in [2]. In general, results have shown that the new model significantly outperforms the models presented in [1] and in [2].

5 Conclusion

The main goal of this thesis is to conceive a new frequency domain sparse channel model and to design a new algorithm in order to improve certain aspects of the classical Orthogonal Matching Pursuit. In this chapter a conclusion is given based on the analysis performed followed by additional guidelines for future work.

5.1 Main Contributions

This research has contributed to the channel estimation field by exploring the role of sparsity. Specifically, this thesis examines the use of compressed sensing in the estimation of highly sparse channels such the UWB ones. A sparse channel estimation approach has been developed based on the sparse frequency domain model of the UWB signals. It has been proposed to exploit the sparse nature of the channel through the use of a new greedy algorithm named extended OMP (eOMP) which is based on the classic OMP. The new eOMP provides lower false path detection probability compared with classical OMP, which also leads to a better TOA estimation, without significant degradation of the channel estimation. From the simulation results carried out in this master thesis, it can be concluded that eOMP reduces the false path detection probability at the expense of a negligible lost in the channel estimation itself. This can be useful in applications where it is required to be sure that a detected path is a true one, e.g in ranging applications where the first path is used to estimate the TOA.

The new frequency domain sparse channel model is compared with two other existing approaches in the literature. The sparse channel estimation problem is faced in [1] under a time domain sparse model point of view. In [1] a suitable dictionary formed by delayed versions of the UWB transmitted pulse is defined in order to better match the UWB signal. However, the spike basis achieves maximal incoherence with the Fourier basis [7] and is for that reason that seems more convenient to work with frequency

domain measurements. In [2] the sparse model is defined in the frequency domain. To ensure that every measurement counts, they propose to pre-modulate the input signal with a spread spectrum sequence before the Fourier transformation. From the analysis performed, it can be concluded that the proposed sparse model can outperform the ones proposed in [1] and in [2].

5.2 Future Work

Sparse channel estimation and Compressed Sensing Theory are hot concepts in communications world. This means that there is much research going on and many issues that remains to be solved. Due to limited time, we have only focussed on UWB channels and we have only studied the OMP as a sparse signal recovery algorithm. However there are many issues that could be subject to further studies which are out of the scope of this thesis.

Moreover, there are several limitations on the assumptions used in this thesis which can be investigated as possible future work. First and foremost, channel characteristics such as pulse distortion must be accounted for in the channel modeling to be realistic. Even worse, in urban centers, the line-of-sight is often blocked by obstacles, and a collected of differently delayed waves is all what is received by a wireless receiver. Another limitation of the assumed model is that it requires the sparse structure of the channel impulse response to remain stable over a certain time scale, which could be easily violated for the channel considered here.

Regarding the sparse signal recovery algorithms, there are some issues to take into account for further research. In general, a drawback of Matching Pursuit algorithms is its greediness. It could happen that MP (MP or any of its variants) initially selects an atom that is not part of the optimal sparse representation; as a result, many of the subsequent atoms selected simply compensate for the poor selection [66]. In a further work, other sparse signal recovery algorithms such BP have to be studied and compared with the proposed eOMP. As it was mentioned in Section 3.3.5, another important shortcoming of iterative algorithms such as MP is the criteria to decide when the algorithm is halted. Here, an heuristic threshold has been used based on the noise energy level. The stopping criteria has an important impact on the final performance of any iterative algorithm and that is why further reserach has to be developed on this point.

UWB has been next year's big technology for five years or so no, but it's starting to look a bit like last year's failure. UWB has never made the kind of breakthrough expected when the technology started to move from theory through regulatory approval and into actual working, shipping silicon. When UWB was first fully realized as the preferred method for personal area networking (PAN) inside the engineering group IEEE's 802.15 PAN group (the 802.15.3a task group), its speed looked like it would be several times higher than anything happening in 802.11; this would make UWB be an effective future direction for the wireless standard to be used by USB. Later, Bluetooth signed on to work with UWB, as well. A big question is: Will ultra-wideband high-speed wireless technology ever find its market?

Fortunately, the UWB technology still has adherents, applications, and purposes for which WiFi won't work, because WiFi isn't meant for simple, ad-hoc networks in which a computer is the hub of interaction.

6

Appendix: Submitted paper ICASSP 2011

The main results in this master thesis dissertation have been submitted to the 36^{th} International Conference on Acoustics, Speech and Signal Processing which will take place at the Prague Congress Centre (PCC), May 22-27, 2011.

The ICASSP meeting is the worlds largest and most comprehensive technical conference focused on signal processing and its applications.

SPARSE CHANNEL ESTIMATION BASED ON COMPRESSED SENSING FOR ULTRA WIDEBAND SYSTEMS

Eva Lagunas[1] *Montse Nájar*[1,2]

[1] Universitat Politècnica de Catalunya (UPC), Department of Signal Theory and Communications, c/ Jordi Girona, 1-3, Barcelona, Spain
[2] Centre Tecnològic de Telecomunicacions de Catalunya (CTTC), Av. Canal Olímpic s/n, Castelldefels (Barcelona), Spain
eva.lagunas@upc.edu, montse.najar@upc.edu

ABSTRACT

Channel estimation for purposes of equalization is a long standing problem in signal processing. Wireless propagation is characterized by sparse channels, that is channels whose time domain impulse response consists of few dominant multipath finguers. This paper examines the use of compressed sensing in the estimation of highly sparse channels. In particular, a new channel sparse model for ultra-wideband (UWB) communication systems based on the frequency domain signal model is presented. A new greedy algorithm named extended OMP (eOMP) is proposed to reduce the false path detection achieved with classical Orthogonal Matching Pursuit (OMP) allowing better TOA estimation.

***Index Terms*— Channel estimation, Ultra WideBand technology, Compressed Sensing.**

1. INTRODUCTION

Reflection, diffraction and scattering from surrounding objects are typical effects suffered by signals while propagate through a wireless channel. Because of these effects, the transmitted signal arrives at the receiver as a superposition of multiple attenuated and delayed copies of the original signal. However, multipath can be seen both as a curse or as a blessing from a communications point of view depending on the amount of CSI available to the system. If the channel characteristics are known at the receiver, it can be effectively use to improve the communications performance.

On another hand, UWB communications [1] has emerged as a promising technology for wireless communications. Designed for low-power, short-range, wireless personal area networks, UWB is the leading technology for freeing people from wires, enabling wireless connection of multiple devices for transmission of high-bandwidth data.

The transmission of ultrashort pulses in UWB leads to several desirable characteristics such as the rich multipath diversity introduced by the large number of propagation paths existing in a UWB channel. The rich multipath coupled with the fine time resolution of UWB create a challenging channel estimation problem. Fortunately, multipath wireless channels tend to exhibit impulse responses dominated by a relatively small number of clusters of significant paths, especially when operating at large bandwidths. Our goal herein is to exploit the sparse structure of the wireless channel impulse reponse in order to improve the channel estimation by means of the emerging CS theory.

CS [2] is a novel sampling paradigm that goes further than Shannon's theorem. The idea is to perfectly recover the signal using far fewer samples of measurements than traditional methods. CS allows to compress the data while is sampled. It originates from the idea that it is not necessary to invest a lot of power into observing the entries of a sparse signal because most of them will be zero.

It is proved that conventional channel estimation methods provide higher errors because they ignore the prior knowledge of the sparseness [3]. The sparse channel estimation problem is faced in [4] under a time domain sparse model point of view. In [4] a suitable dictionary formed by delayed versions of the UWB transmitted pulse is defined in order to better match the UWB signal. However, the spike basis achieves maximal incoherence with the Fourier basis [5] and is for that reason that seems more convenient to work with frequency domain measurements. In [6] the sparse model is defined in the frequency domain. To ensure that every measurement counts, they propose to pre-modulate the input signal with a spread spectrum sequence before the Fourier transformation.

Here, a sparse channel estimation approach is developed based on the sparse frequency domain model of the UWB signals without pre-modulation. We propose exploiting the sparse nature of the channel through the use of a new greedy algorithm named extended OMP (eOMP) in order to reduce the false path detection probability achieved with classical OMP and to derive an improved TOA estimation. The performance of the new model is compared with [4] and [6].

The reminder of this paper is as follows: Section II describes the classic UWB signal model. In Section III the sparse frequency domain model is formulated and the extended OMP (eOMP) is introduced. Simulation results of the new model and comparations with the previous work in the literature are given in Section IV. Finally, conclusions are drawn in Section V.

2. UWB SIGNAL MODEL

The transmitted UWB signal model can be written as,

$$s(t) = \sum_{k=0}^{\infty} \sum_{j=0}^{N_f-1} a_k p(t - jT_f - kT_{sym}) \quad (1)$$

where the data $a_k \in \pm 1$ is the k-th transmitted bit, T_{sym} is the symbol duration and $T_f = T_{sym}/N_f$ is the pulse repetition period. To simplify notation, in the following it is assumed $a_k = 1$.

This work was partially supported by the Catalan Government under grant 2009 SGR 891, by the Spanish Government under project TEC2008-06327- C03 (MULTI-ADAPTIVE) and by the European Commission under project NEWCOM++ (ICT-FP7-216715).

E. Lagunas was supported by the Catalan Government under grant FI-DGR 2010.

Signal $s(t)$ propagates through an L-path fading channel whose response to $p(t)$ is $\sum_{l=0}^{L-1} h_l p(t-\tau_l)$. The received waveform can be written as

$$r(t) = \sum_{k=0}^{\infty} \sum_{j=0}^{N_f-1} \sum_{l=0}^{L-1} h_l p(t - T_k^j - \tau_l) + w(t) \tag{2}$$

where $w(t)$ is thermal noise with two-sided power spectral density $No/2$ and $T_k^j = jT_f + kT_{sym}$. The signal associated to the j-th transmitted pulse corresponding to the k-th symbol, in the frequency domain yields

$$Y_j^k(w) = \sum_{l=0}^{L-1} h_l S_j^k(w) e^{-jw\tau_l} + V_j^k(w) \tag{3}$$

with

$$S_j^k(w) = P(w) e^{-jw(kN_f+j)T_f} \tag{4}$$

where $P(w)$ denotes the Fourier Transform of the pulse $p(t)$ and $V_j^k(w)$ is the noise in the frequency domain associated to the j-th frame interval correspondig to the k-th symbol. Sampling (3) at $w_m = w_0 m$ for $m = 0, 1, \ldots, M-1$ where $w_0 = \frac{2\pi}{T_f}$ and rearranging the frequency domain samples $Y_j^k[m]$ into the vector $\mathbf{Y}_j^k \in \mathbb{C}^{M\times 1}$ yields

$$\mathbf{Y}_j^k = \sum_{l=0}^{L-1} h_l \mathbf{S}_j^k \mathbf{e}_{\tau_l} + \mathbf{V}_j^k = \mathbf{S}_j^k \mathbf{E}\mathbf{h} + \mathbf{V}_j^k \tag{5}$$

where the matrix $\mathbf{S}_j^k \in \mathbb{C}^{M\times M}$ is a diagonal matrix whose components are the frequency samples of $S_j^k(w)$ and the matrix $\mathbf{E} \in \mathbb{C}^{M\times L}$ contains the delay-signature vectors associated to each arriving delayed signal

$$\mathbf{E} = \begin{bmatrix} \mathbf{e}_{\tau_0} & \ldots & \mathbf{e}_{\tau_l} & \ldots & \mathbf{e}_{\tau_{L-1}} \end{bmatrix} \tag{6}$$

with $\mathbf{e}_{\tau_l} = \begin{bmatrix} 1 & e^{-jw_0\tau_l} & \ldots & e^{-jw_0(M-1)\tau_l} \end{bmatrix}^T$. The channel fading coefficients are arranged in the vector $\mathbf{h} = \begin{bmatrix} h_0 & \ldots & h_{L-1} \end{bmatrix}^T \in \mathbb{R}^{L\times 1}$, and the noise samples in vector $\mathbf{V}_j^k \in \mathbb{C}^{M\times 1}$.

3. EXTENDED OMP IN FREQUENCY DOMAIN

A proper sparse representation of the channel is required in order to easily apply the CS theory. A tutorial overview of some of the basic developments in CS can be found in [5]. The expression in (5) free of noise can be extended and reformulated as,

$$\mathbf{Y}_j^k = \mathbf{B}_j^k \mathbf{h}_e = \mathbf{S}_j^k \mathbf{E}_e \mathbf{h}_e \tag{7}$$

The main difference between (7) and (5) is the extended matrix $\mathbf{E}_e$, which is an $M \times M$ extended delay-matrix which contains not only the L delay-signature vectors corresponding to the multipath, but also $M-L$ delay-signature vectors with no channel contribution (see Fig. 1). Therefore, vector $\mathbf{h}_e$ is an *L-sparse* vector whose elements different from zero correspond to the original channel coefficients, that is, calling $\mathbf{e}_{\tau_m}$ the m-th column of $\mathbf{E}_e$, when

$$\mathbf{e}_{\tau_m} = \mathbf{e}_{\tau_l} \quad \text{for } l = 0, \ldots, L-1 \tag{8}$$

Note that the dimension M will determine the path resolution.

In a typical CS notation, $\mathbf{h}_e$ can be identified as the *L-sparse* vector and $\mathbf{B}_j^k$ as the dictionary where the channel becomes sparse.

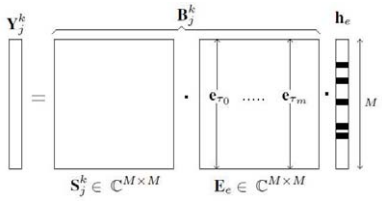

Fig. 1. Sparse Sructure of the channel

In order to compress the frequency domain samples a widely used random matrix $\mathbf{C}_f \in \mathbb{R}^{N\times M}$ with entries i.i.d. taken from a normal distribution with zero-mean and unit variance is used.

$$\mathbf{Y}_c = \mathbf{C}_f \mathbf{Y}_j^k = \mathbf{C}_f \mathbf{B}_j^k \mathbf{h}_e \tag{9}$$

where $\mathbf{Y}_c$ is the $N \times 1$ vector of measurements. $\mathbf{C}_f$ is known as measurement matrix and it has rank N lesser than the rank of the signal which is equal to M. Thus, the $N \times M$ matrix $\mathbf{C}_f$ is projecting the signal $\mathbf{Y}_j^k$. Randomness in the measurement matrix can lead to a very efficient sensing mechanisms. It has been shown that random matrices are largely incoherent with any fixed basis (which is one of the principles of CS).

Therefore, the sparse channel estimation $\hat{\mathbf{h}}_e$ can be obtained from the compressed samples $\mathbf{Y}_c$ applying sparse signal reconstruction techniques. The sparse signal reconvery problem is formulated as,

$$\min_{\hat{\mathbf{h}}_e \in \mathbb{R}^M} \left\| \hat{\mathbf{h}}_e \right\|_{l_1} \quad s.t. \quad \mathbf{Y}_c = \mathbf{C}_f \mathbf{B}_j^k \hat{\mathbf{h}}_e \tag{10}$$

where $\left\| \hat{\mathbf{h}}_e \right\|_{l_1} = \sum_{i=1}^{M} \left| \hat{h}_e(i) \right|$. Note that the only prior knowledge required is that $\mathbf{h}_e$ is sparse. Reconstruction then only requires the space in which the signal is sparse.

There are many approaches discussed in literature for solving (10). Currently, the two most popular approaches are matching pursuit (MP) [7] and basis pursuit (BP) [8]. With MP (and one of its variants OMP) the sparse signal is iteratively built up by selecting the atom that maximally improves the representation at each iteration. On the other hand, BP directly looks for the vector that minimize the l_1-norm coefficients, which is computationally expensive. Here, OMP [9] is used to achieve faster and more efficient reconstruction. However, imperfections between the assumed model and the received signal can cause false path detection. This false path detection leads to a wrong TOA estimation. To improve the TOA estimation but preserving the performance of channel estimator it is proposed an extended OMP (eOMP) (Algorithm 1). Both OMP and eOMP are iterative greedy algorithms that select at each step the dictionary element best correlated with the residual part of the signal. Then they produce a new approximation by projecting the signal onto the dictionary elements that have already been selected. The main difference between OMP and eOMP is that eOMP not only pick the column of the dictionary that is most strongly correlated but also the $2k+1$ neighbors of it. To obatin the final values of the non-zero elements of the sparse vector the same step with only the most strongly correlated element is computed in parallel.

Algorithm 1 eOMP

Input

$(\cdot)$ An $N \times M$ matrix $\mathbf{C}_f\mathbf{B}_j^k$ which columns are expressed as φ_j

$(\cdot)$ An N dimensional data vector $\mathbf{Y}_c$

$(\cdot)$ An energy threshold

$(\cdot)$ Number of neighbors k (related to the pulse duration and the channel estimation resolution)

Procedure

(1) Initialize the residual $\mathbf{r}_0 = \mathbf{Y}_c$, the index sets $\Lambda_0 = \emptyset$ and $\Lambda_0^e = \emptyset$, and the iteration counter $t = 1$.

(2) Find the index λ_t that solves the easy optimization problem

$$\lambda_t = \arg \max_{j=1,\ldots,N} |\langle \mathbf{r}_{t-1}, \varphi_j \rangle|$$

(3) Augment the extended and non-extended index set and the extended and non-extended matrix of chosen atoms:

$$\Lambda_t^e = \Lambda_{t-1}^e \cup \{\lambda_t - k\} \cup \ldots \cup \{\lambda_t\} \cup \ldots \cup \{\lambda_t + k\}$$

$$\Phi_t^e = [\Phi_{t-1}^e \;\; \varphi_{\lambda_t - k} \;\; \cdots \;\; \varphi_{\lambda_t} \;\; \cdots \;\; \varphi_{\lambda_t + k}]$$

$$\Lambda_t = \Lambda_{t-1} \cup \{\lambda_t\}$$

$$\Phi_t = [\Phi_{t-1} \;\; \varphi_{\lambda_t}]$$

We use the convention that Φ_0 and Φ_0^e are empty matrices.

(4) Solve the least square problem to obtain a new signal estimate

$$\mathbf{x}_t^e = \arg\min_{\mathbf{x}} \|\mathbf{Y}_c - \Phi_t^e \mathbf{x}\|_2$$

$$\mathbf{x}_t = \arg\min_{\mathbf{x}} \|\mathbf{Y}_c - \Phi_t \mathbf{x}\|_2$$

(5) Calculate the new approximation of the data and the new residual

$$\mathbf{a}_t = \Phi_t^e \mathbf{x}_t^e$$

$$\mathbf{r}_t = \mathbf{Y}_c - \mathbf{a}_t$$

(6) Increment t, and return to Step 2 if the energy threshold is not achieved.

(7) The estimate $\hat{\mathbf{h}}_e$ for the ideal signal has nonzero indices at the components listed in Λ_t and the value of the estimate $\hat{\mathbf{h}}_e$ in component λ_j equals the j-th component of $\mathbf{x}_t$.

$$\hat{\mathbf{h}}_e(\Lambda_t) = \mathbf{x}_t$$

4. SIMULATION RESULTS

For numerical evaluation of the algorithm we consider the channel models developed within the framework of the IEEE 802.15.4a. In particular it is used the CM1 Residential LOS channel model. All simulations are given for 100 independent channel realizations. M is fixed at 768 and the compression rate is expressed with $\rho = \frac{N}{M}$ (meaning $\rho << 1$ high undersampling). The pulse duration is equal to 0.77ns (which theoreticaly correspond to a Nyquist compression when $\rho = 0.33$). The number of multipath components L that form the UWB channel can be quite large, however many of those paths are negligible. Therefore, we limit ourselves to estimate the L_c most significant paths which are the ones capturing 80% of the channel energy.

The quality of the channel estimation is evaluated with the RMSE computed as,

$$RMSE = \frac{1}{M}\mathbf{e}^H\mathbf{e} \tag{11}$$

where the error $\mathbf{e}$ is defined as,

$$\mathbf{e} = \mathbf{ifft}(\mathbf{B}_f^k \hat{\mathbf{h}}_e) - \mathbf{r}_{wn} \tag{12}$$

with $\mathbf{r}_{wn}$ being the received signal without noise.

Fig. 2 depicts the TOA estimation expressed in meters using OMP and eOMP with k=2. It is shown that the new eOMP outperforms the classical OMP without degrading the RMSE of the channel estimation (Fig. 3).

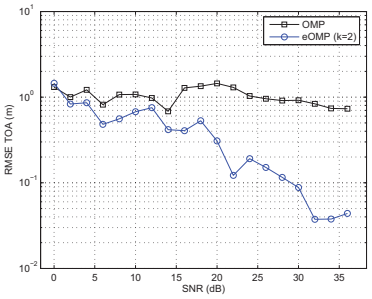

Fig. 2. TOA estimation for $\rho = 0.167$

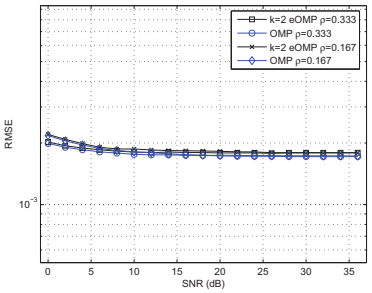

Fig. 3. RMSE of the sparse channel estimation

Fig. 4 depicts the false path detection probability using OMP and eOMP. The results are also compared for different compression rates. Results shown that the new eOMP reduces the false alarm probability. In both cases, performance is slightly worse as the compression rate decrease.

From now on, eOMP will be used in future simulations.

The perfomance is compared with the time domain sparse model proposed in [4] where the dictionary used is a circulant matrix $\mathbf{P} \in \mathbb{R}^{M \times M}$ whose columns are shifted replicas of the mother pulse $p(t)$. The compressed samples are obtained with a random measurement matrix as in (9),

$$\mathbf{y}_c = \mathbf{C}_t \mathbf{P} \hat{\mathbf{h}}_e \tag{13}$$

where $\mathbf{C}_t \in \mathbb{R}^{N \times M}$. In this case the RMSE is obtained with the following error definition,

$$\mathbf{e} = \mathbf{P}\hat{\mathbf{h}}_e - \mathbf{r}_{wn} \tag{14}$$

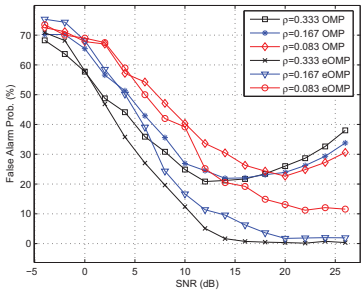

Fig. 4. False path detection probability for different compression rates

Fig. 5 depicts the RMSE of the recovered signal using the channel estimation presented here compared with [4]. At the Nyquist compression rate, the RMSE remains the same for both approaches. But as the compression rate decrease, the errors in the time domain increase more than in the frequency domain for high SNR.

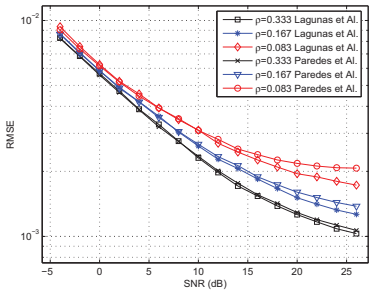

Fig. 5. RMSE of the recovered signal compared with the time domain approach in [4]

A comparison with another frequency domain model presented in [6] has been done. In [6], the spectrum is spread pre-modulating the input signal with a pseudorandom sequence $p[n]$ before the Fourier transformation ensuring that every measurement carries information,

$$\mathbf{y}_c = \mathbf{RF}\mathrm{diag}(p[n])\mathbf{Ph}_e \tag{15}$$

where $\mathbf{F}$ is the column normalized DFT matrix and $\mathbf{R}$ is the subsampling operator. Therefore $\mathbf{RF}$ is simply standard Fourier subsampling matrix.Results depicted in Fig. 6 show that the estimation error with the new model outperforms [6] whatever the compression rate is.

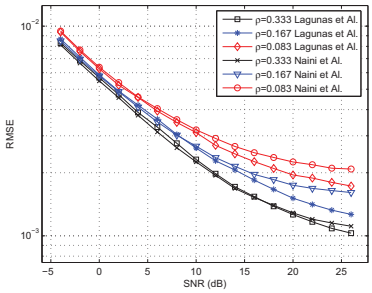

Fig. 6. RMSE of the recovered signal compared with the approach in [6]

5. CONCLUSIONS

A frequency domain UWB sparse channel estimator based on CS theory has been presented and a new algorithm named eOMP is proposed. Simulation proved that eOMP improve the classical OMP TOA estimation. Simulation results carried out with eOMP have shown that the new sparse channel model can outperform other models presented in [4] and [6] for high SNR and for high compression rates.

6. REFERENCES

[1] X. Shen, M. Guizani, H. Chen, R. C. Qiu, and A. Molisch, "Ultra-Wideband Wireless Communications," *IEEE J. Select. Areas Commun*.

[2] D.L. Donoho, "Compressed Sensing," *IEEE Trans. Information Theory*, vol. 52, no. 4, pp. 1289–1306, Apr, 2006.

[3] F. Wan, W. P. Zhu, and M. N. S. Swamy, "Semi-Blind Most Significant Tap Detection for Sparse Channel Estimation of ofdm Systems," *IEEE Trans. Circuits and Systems*.

[4] J. L. Paredes, G. R. Arce, and Z. Wang, "Ultra-Wideband Compressed Sensing: Channel Estimation," *IEEE J. Select. Top. Signal Processing*, vol. 1, no. 3, pp. 383–395, Oct, 2007.

[5] E. J. Candes and M. B. Wakin, "An Introduction to Compressed Sampling," *IEEE Signal Processing Magazine*, vol. 25, no. 2, pp. 21–30, March, 2008.

[6] F.M. Naini, R. Gribonval, L. Jacques, and P. Vandergheynst, "Ultra-Wide Bandwidth Time-Hopping Spread-Spectrum Impulse Radio for Wireless Multiple-Acces Communications," *IEEE ICASSP*, pp. 2877–2880, 2009.

[7] S. G. Mallat and Z. Zhang, "Matching Pursuits with Time-Frequency Dictionaries," *IEEE Trans. Signal Processing*, vol. 41, no. 12, pp. 3397–3415, Dec, 1993.

[8] S. S. Chen, D. L. Donoho, and M. A. Saunders, "Atomic Decomposition by Basis Pursuit," *Society for Industrial and Applied Mathematics Review*, vol. 43, no. 1, pp. 129–159, 2001.

[9] J. A. Tropp and A. C. Gilbert, "Signal Recovery From Random Measurements Via Orthogonal Matching Pursuit," *IEEE Trans. Information Theory*, vol. 53, no. 12, pp. 4655–4666, Dec, 2007.

References

[1] J. L. Paredes, G. R. Arce, and Z. Wang, "Ultra-Wideband Compressed Sensing: Channel Estimation," *IEEE Journal of Selected Topics in Signal Processing*, vol. 1, no. 3, pp. 383–395, Oct, 2007.

[2] F. Naini, R. Gribonval, L. Jacques, and P. Vandergheynst, "Ultra-Wide Bandwidth Time-Hopping Spread-Spectrum Impulse Radio for Wireless Multiple-Acces Communications," *IEEE International Conference on Acoustics, Speech and Signal Processing*, pp. 2877–2880, Apr, 2009.

[3] S. S. Chen, D. L. Donoho, and M. A. Saunders, "Atomic Decomposition by Basis Pursuit," *SIAM Journal on Scientific Computing*, vol. 20, no. 1, pp. 33–61, 1999.

[4] M. Win and R. Scholtz, "Ultra-Wide Bandwidth Time-hopping Spread Spectrum Impulse Radio for Wireless Multiple-access Communications," *IEEE Transactions on Communications*, vol. 48, pp. 679–689, April, 2000.

[5] A. Saleh and R. Valenzuela, "A Statistical Model for Indoor Multipath Propagation," *IEEE Journal on Selected Areas Communications*, pp. 128–137, Feb, 1987.

[6] D. Donoho, "Compressed Sensing," *IEEE Transactions on Information Theory*, vol. 52, no. 4, pp. 1289–1306, Apr, 2006.

[7] E. J. Candes and M. B. Wakin, "An Introduction to Compressed Sampling," *IEEE Signal Processing Magazine*, vol. 25, no. 2, pp. 21–30, March, 2008.

[8] J. A. Tropp and A. C. Gilbert, "Signal Recovery From Random Measurements Via Orthogonal Matching Pursuit," *IEEE Transactions on Information Theory*, vol. 53, no. 12, pp. 4655–4666, Dec, 2007.

[9] M. Unser, "Sampling: 50 Years After Shannon," *Procedings of the IEEE*, vol. 88, no. 4, pp. 569–587, 2000.

[10] E. J. Candes and T. Tao, "Near Optimal Signal Recovery from Random Projections: Universal Encoding Strategies," *IEEE Transactions on Information Theory*, vol. 52, no. 12, pp. 5406–5425, Dec, 2006.

[11] D. Taubman and M. Marcellin, *JPEG−2000: Image Compression Fundamentals, Standards and Practice*. Kluwert Academic Publishers, 2001.

[12] R. Cramer, R. Scholtz, and M. Win, "Evaluation of an Ultra-Wide-Band Propagation Channel," *IEEE Transactions on Antennas and Propagation*, vol. 50, no. 5, pp. 561–570, May, 2002.

[13] M. Rudelson and R. Vershynin, "On Sparse Reconstruction from Fourier and Gaussian Measurements," *Communications on Pure and Applied Mathematics*, vol. 61, no. 8, pp. 1025–1045, 2008.

[14] E. J. Candes, "Compressive Sampling," *Proceedings of the International Congress of Mathematicians (ICM)*, vol. 3, pp. 1433–1452, 2006.

[15] J. Tropp, "Just Relax: Convex Programming Methods for Identifying Sparse Signals," *IEEE Transactions on Information Theory*, vol. 52, no. 3, pp. 1030–1051, Mar, 2006.

[16] E. J. Candes, J. Romberg, and T. Tao, "Stable Signal Recovery from Incomplete and Inaccurate Measurements," *Communications on Pure and Applied Mathematics*, vol. 59, no. 8, pp. 1207–1223, 2006.

[17] S. Boyd and L. Vandenberghe, *Convex Optimization*. Cambridge University Press, 2004.

[18] J. A. Tropp, "Greed is Good: Algorithmic Results for Sparse Approximation," *IEEE Transactions on Information Theory*, vol. 50, no. 10, pp. 2231–2242, Oct, 2004.

[19] J. Tropp and D. Needell, "CoSaMP: Iterative Signal Recovery from Incomplete and Inaccurate Samples," *Applied and Computational Harmonic Analysis*, vol. 26, no. 3, pp. 301–321, Apr, 2008.

[20] F. Bergeaud and S. Mallat, "Matching Pursuit of Images," *Int. Conf. on Image Processing*, p. 53, 1995.

[21] P. Phillips, "Matching Pursuit Filters applied to Face Identification," *IEEE Transactions on Image Processing*, vol. 7, no. 8, pp. 1150–1164, Aug, 1998.

[22] E. J. Candes and T. Tao, "The Dantzig Selector: Statistical Estimation when p is much larger than n," *Annals of Statistics*, vol. 35, no. 6, pp. 2313–2351, Dec, 2007.

[23] J. Haupt and R. Nowak, "Signal Reconstruction from Noisy Random Projections," *IEEE Transactions on Information Theory*, vol. 52, no. 9, pp. 4036–4048, 2006.

[24] R. Tibshirani, "Regression Shrinkage and Selection via the Lasso," *Journal of the Royal Statistical Society*, vol. 58, no. 1, pp. 267–288, 1996.

[25] M. S. Asif, "Primal Dual Pursuit: A Homotopy Based Algorithm for the Dantzig Selector," Master's thesis, Georgia Institute of Technology, Atlanta, EEUU, 2008.

[26] S. Pfetsch, T. Ragheb, J. Laska, H. Nejati, A. Gilbert, M. Strauss, R. Baraniuk, and Y. Massoud, "On the Feasibility of Hardware Implementation of Sub-Nyquist Random-Sampling Based Analog-to-Information Conversion," *IEEE International Symposium on Circuits and Systems*, pp. 1480–1483, May, 2008.

[27] S. Kirolos, J. Laska, M. Wakin, M. Duarte, D. Baron, T. Ragheb, Y. Massoud, and R. Baraniuk, "Analog-to-Information Conversion via Random Demodulation," *IEEE Dallas/CAS Workshop on Design, Applications, Integration and Software*, pp. 71–74, Oct, 2006.

[28] "First Report and Order 02-48," tech. rep., Federal Communications Commission, Feb, 2002.

[29] "Comission decision of 21 February 2007 on allowing the use of the radio spectrum for equipment using UWB technology in a harmonised manner in the community (2007/131/EC)," tech. rep., Comission of the European Communities, Feb, 2002.

[30] M. Ghavami, L. Michael, and R. Kohno, *Ultra WideBand: Signals and Systems in Communication Engineering*. John Wiley and Sons, 2007.

[31] R. Scholtz, "Multiple Access with Time-Hopping Impulse Modulation," *IEEE Military Communications Conference*, pp. 447–450, 1993.

[32] M. Z. Win and R. A. Scholtz, "Characterization of Ultra-Wide bandwidth Wireless Indoor Channels: A communications-theoretic view," *IEEE Journal on Selected Areas Communications*, vol. 20, no. 9, pp. 1613–1627, 2002.

[33] V. Lottici, A. D'Andrea, and U. Mengali, "Channel Estimation for Ultra-Wideband Communications," *IEEE Journal on Selected Areas Communications*, vol. 20, no. 9, pp. 1638–1645, 2002.

[34] I. Guvenc and Z. Sahinoglu, "Threshold-based TOA Estimation for Impulse Radio UWB Systems," *IEEE International Conference on UWB*, pp. 420–425, Sept, 2005.

[35] R. Harjani, J. Harvey, and R. Sainati, "Analog/RF physical layer issues for UWB systems," *17th International Conference VLSI Design, Mumbai, India*, pp. 941–948, 2004.

[36] M. Mielczarek, M. Wessman, and U. Mitra, "Performance of coherent UWB rake receiver with channel estimators," *IEEE Vehicular Technology Conference, Orlando, FL*, pp. 1880–1884, Oct, 2003.

[37] C. Carbonelli, U. Mengali, and U. Mitra, "Synchronization and Channel Estimation for UWB signals," *Global Telecommunications Conference, San Francisco, CA*, pp. 764–768, 2003.

[38] C. Carbonelli, S. Vedantam, and U. Mitra, "Sparse Channel Estimation with Zero Tap Detection," *International Conference on Communications, Paris, France*, pp. 3173–3177, Jun, 2004.

[39] C. Carbonelli and U. Mengali, "M-PPM noncoherent receivers for UWB applications," *IEEE Transactions on Wireless Communications*, vol. 5, no. 8, pp. 2285–2294, 2006.

[40] X. Dong, L. Jin, and P. Orlik, " New Transmitted Reference Pulse Cluster System for UWB Communications," *IEEE Transactions on Vehicular Technology*, vol. 57, no. 5, pp. 3217–3224, 2008.

[41] X. Wang, G. Arce, B. Sadler, J. Paredes, and X. Ma, "Compressed Detection for Pilot Assisted Ultra-Wideband Impulse Radio," *IEEE International Conference on UWB*, pp. 393–398, Sept, 2007.

[42] A. Goldsmith, *Wireless Communications*. Cambridge University Press, 2005.

[43] L. Tong, B. M. Sadler, and M. Dong, "Pilot-Assisted Wireless Transmissions," *IEEE Signal Processing Magazine*, vol. 21, no. 6, pp. 12–25, Nov, 2004.

[44] L. Tong and S. Perreau, "Multichannel Blind Identification: From Subspace to Maximum Likelihood Methods," *Procedings of the IEEE*, vol. 86, no. 10, pp. 1951–1968, Oct, 1998.

[45] A. F. Molisch, "Ultrawideband Propagation Channels: Theory, Measurement and Modeling," *IEEE Transactions on Vehicular Technology*, vol. 54, no. 5, pp. 1528–1545, Sep, 2005.

[46] N. Czink, X. Yin, H. Ozcelik, M. Herdin, E. Bonek, and B. H. Fleury, "Cluster Characteristics in a MIMO Indoor Propagation Enviroment," *IEEE Transactions on Wireless Communications*, vol. 6, no. 4, pp. 1465–1475, Apr, 2007.

[47] F. Wan, W. P. Zhu, and M. N. S. Swamy, "Semi-Blind Most Significant Tap Detection for Sparse Channel Estimation of ofdm Systems," *IEEE Transactions on Circuits and Systems Part I: Regular Papers*, vol. 57, no. 3, pp. 703–713, Mar, 2010.

[48] S. G. Mallat and Z. Zhang, "Matching Pursuits with Time-Frequency Dictionaries," *IEEE Transactions on Signal Processing*, vol. 41, no. 12, pp. 3397–3415, Dec, 1993.

[49] M. R. Raghavendra and K. Giridhar, "Improving Channel Estimation in OFDM Systems for Sparse Multipath Channels," *IEEE Signal Processing Letters*, vol. 12, no. 1, pp. 52–55, Jan, 2005.

[50] "802.15.4a-2007: IEEE Standard for Information Technology - Telecommunications and information exchange between systems - Local and metropolitan area networks - specific requirement. Part 15.4: Wireless Medium Access Control

(MAC) and Physical Layer (PHY) Specifications for Low-Rate Wireless Personal Area Networks (WPANs)," 2007.

[51] A. Rontogiannis and K. Berberidis, "Bandwidth Efficient Transmission through Sparse Channel using Parametric Channel-Estimation-Based DFE," *Proc. Inst. Electr. Eng. Commun.*, vol. 152, no. 2, pp. 251–256, 2005.

[52] D. L. Donohon and M. Elad, "Optimally Sparse Representation in General (nonoorthogonal) Dictionaries via L1 minimization," *Proc. National Academy of Science of the USA*, vol. 100, no. 5, pp. 2197–2202, Mar, 2003.

[53] Y. C. Pati, R. Rezaiifar, and P. S. Krishnaprasad, "Orthogonal Matching Pursuit: Recursive Function Approximation with Applications to Wavelet Decomposition," 27^{th} *Asilomar Conference on Signals, Systems and Computers*, vol. 1, pp. 40–44, Nov, 1993.

[54] D. Donoho, Y. Tsaig, and I. Drori, "Sparse Solution of Under-Determined Linear Equations of Stagewise Orthogonal Matching Pursuit," *Technical Report, Department of Statistics, Stanford University*, 2006.

[55] S. Cotter and B. Rao, "Application of Tree-Based Searches to Matching Pursuit," *International Conference on Acoustics, Speech and Signal Processing (ICASSP), USA*, pp. 3933–3936, 2001.

[56] P. Jost and P. Vandergheynst, "Tree-Based Pursuit: Algorithm and Properties," *IEEE Transactions on Signal Processing*, vol. 54, no. 12, pp. 4685–4697, 2006.

[57] G. Davis, S. Mallat, and M. Avellaneda, "Greedy Adaptive Approximation," *Constructive Approximation*, vol. 13, no. 1, pp. 57–98, 1997.

[58] R. DeVore, "Nonlinear approximation," *Acta Numerica*, pp. 51–150, 1998.

[59] V. Temlyakow, "Nonlinear Methods of Approximation," *Foundations of Comput. Math.*, vol. 5, Jul, 2002.

[60] J. H. Gross and D. M. Etter, "Comparison of Echo Cancellation Algorithms for the Adaptive Delay Filter," *IEEE Transactions on Vehicular Technology*, vol. 1, pp. 574–576, May, 1992.

[61] A. Sugiyama, H. Sato, A. Hirano, and S. Ikeda, "A fast Convergence Algorithm for Adaptive FIR Filters under Computational Constraint for Adaptive Tap-Position Control," *IEEE Transactions on Circuits and Systems II*, vol. 43, no. 9, pp. 629–636, Sep, 1996.

[62] J. Tropp, "Average-Case Analysis of Greedy Pursuit," *Proc. SPIE Wavelets XI (Invited Paper)*, vol. 5914, Aug, 2005.

[63] D. Donoho and J. Tanner, "Precise Undersampling Theorems," *Proceedings of the IEEE*, vol. 98, no. 6, pp. 913–924, May, 2010.

[64] Y. C. Eldar, "Analog Compressed Sensing," *IEEE International Conference on Acoustics, Speech and Signal Processing*, pp. 2949–2952, Apr, 2009.

[65] M. Mishali and Y. C. Eldar, "From Theory to Practice: Sub-Nyquist sampling of Sparse Wideband Analog Signals," *IEEE Journal of Selected Topics on Signal Processing*, vol. 4, no. 2, pp. 375–391, Apr, 2010.

[66] R. DeVore and V. Temlyakow, "Some Remarks on Greedy Algorithms," *Advances in Computational Mathematics*, vol. 5, pp. 173–187, 1996.